

Free Privacy Protection for Wireless Federated Learning: Enjoy It or Suffer from It?

Weicai Li, *Graduate Student Member, IEEE*, Tiejun Lv, *Senior Member, IEEE*,
Xiyu Zhao, Xin Yuan, and Wei Ni

Abstract—Inherent communication noises have the potential to preserve privacy for wireless federated learning (WFL) but have been overlooked in digital communication systems predominantly using floating-point number standards, *e.g.*, IEEE 754, for data storage and transmission. This is due to the potentially catastrophic consequences of bit errors in floating-point numbers, *e.g.*, on the sign or exponent bits. This paper presents a novel channel-native bit-flipping differential privacy (DP) mechanism tailored for WFL, where transmit bits are randomly flipped and communication noises are leveraged, to collectively preserve the privacy of WFL in digital communication systems. The key idea is to interpret the bit perturbation at the transmitter and bit errors caused by communication noises as a bit-flipping DP process. This is achieved by designing a new floating-point-to-fixed-point conversion method that only transmits the bits in the fraction part of model parameters, hence eliminating the need for transmitting the sign and exponent bits and preventing the catastrophic consequence of bit errors. We analyze a new metric to measure the bit-level distance of the model parameters and prove that the proposed mechanism satisfies (λ, ϵ) -Rényi DP and does not violate the WFL convergence. Experiments validate privacy and convergence analysis of the proposed mechanism and demonstrate its superiority to the state-of-the-art Gaussian mechanisms that are channel-agnostic and add Gaussian noise for privacy protection.

Index terms— Wireless federated learning, differential privacy, floating-point number, communication error, bit-flipping.

I. INTRODUCTION

Privacy-preserving federated learning (FL) integrates privacy models into a distributed machine learning (ML) framework, offering provable privacy assurances [1]–[5]. Differential privacy (DP) is prevalent with several variants studied extensively, including ϵ -DP [6], (ϵ, δ) -DP [7], Rényi DP [8], and (λ, ϵ) -Rényi DP [8]–[10]. Combining DP with FL permits clients to train their local models within specified privacy protection levels [11], [12]. Existing privacy-preserving mechanisms, *e.g.*, Gaussian mechanism [10], [13]–[15] and Laplace mechanism [10], [15], typically add artificial DP noise to the

(decimal) local model parameters at the clients' side before digitizing and uploading them to a server.

Motivation. Wireless channels are noisy and prone to errors due to various factors like thermal noise—also known as Johnson-Nyquist noise—which results from the random movement of electrons in electronic circuits and cannot be entirely eliminated [16]. Nevertheless, the communication noises and their resulting errors may offer an unexpected benefit for privacy protection in wireless FL (WFL).

Both the benefits of leveraging communication noises for preserving the privacy of WFL and the consequences of not doing so are obvious. On the one hand, a limited amount of communication errors in the received local models can be tolerated to enhance privacy preservation, as shown in over-the-air (OTA) FL [13], [17]. By tolerating such errors, more local models with tolerable, mild errors can be aggregated within the available time and spectrum resources, compared to conventional methods that discard erroneous packets or wait for retransmissions [14], [18]. On the other hand, if the privacy-preserving potential of noisy wireless channels is overlooked, unnecessarily tight privacy budgets and high DP noises would be required, thus hindering the convergence of WFL. In this sense, WFL either enjoys the inherent privacy protection offered by noisy wireless channels, or suffers from ineffective communication resource utilization and penalized convergence and accuracy.

No existing studies have exploited the inherent privacy protection offered by noisy wireless channels in digital communication systems. The authors of [13], [17], [19] proposed a privacy-preserving over-the-air (OTA) FL system that leverages communication noise to enhance privacy under analog communication settings. However, implementing such an analog approach would face practical challenges, including high noise sensitivity and low spectrum efficiency, which have driven the global transition from analog communication to digital transmission (*e.g.*, cellular networks, broadcasting, etc.). The authors of [20] introduced a bit-aware randomized response mechanism for local differential privacy. Considering that different bits have different impacts on embedded features, the mechanism heuristically assigns the bits with more significance with smaller randomization probabilities. However, communication noise is generally assumed to impact all transmitted bits uniformly, meaning each bit has an equal probability of being flipped.

Research Challenges. It is non-trivial to exploit the communication noises for the privacy of WFL in digital communication systems due to the predominant use of floating-

Manuscript received 24 July 2024; revised 06 February 2025, 03 May 2025, and 11 June 2025; accepted 12 June 2025. This paper was supported in part by the National Natural Science Foundation of China under No. 62271068, and the Beijing Natural Science Foundation under Grant No. L222046. (*corresponding author: Tiejun Lv.*)

W. Li, T. Lv, and X. Zhao are with the School of Information and Communication Engineering, Beijing University of Posts and Telecommunications, Beijing 100876, China. W. Li is also with the University of Technology Sydney, Broadway, NSW, Sydney. X. Zhao is also with Macquarie University, Macquarie Park, NSW, Sydney. (e-mail: {liweicai, lvtiejun, zxy}@bupt.edu.cn).

X. Yuan is with Tongji University, Shanghai 201804, China.

W. Ni is with Macquarie University, Macquarie Park, NSW 2109, Australia.

point number standards, *e.g.*, IEEE 754 [21]. In practice, data and information are stored and transmitted in bits following the floating-point number standards, which necessitate fidelity during data storage and transmission. For example, the IEEE 754 floating-point standard [21] encodes every number into bits with varying levels of significance, including a sign bit, exponent bits, and fraction bits. A single error in the sign or exponent bits can drastically distort the value. To this end, WFL, when adhering to current practical floating-point standards as implicitly assumed in existing FL designs [14], [15], neither tolerates communication errors nor facilitates the exploitation of communication noise for privacy protection. Moreover, it is challenging to determine the sensitivity and subsequently the privacy budget of the bitstreams, *e.g.*, IEEE 754 floating-point numbers. The reason is that two bitstreams can represent similar (decimal) values but differ dramatically in bits. Exploiting communication noises for privacy protection in WFL requires careful consideration of these factors to balance error tolerance with meaningful privacy benefits.

Contribution. This paper presents a novel *channel-native bit-flipping DP mechanism* tailored for WFL in digital communication systems using floating-point standards. By integrating both artificial and communication noises at the bit level, this mechanism ensures compliance with (λ, ϵ) -Rényi DP, thereby bolstering the privacy of WFL. We provide a comprehensive analysis of the statistical properties of bit-flipping noise and its impact on the convergence of WFL.

The proposed mechanism offers privacy-by-design WFL through its compatibility with digital systems and by exploiting the inherent privacy-preserving properties of noisy wireless channels. The mechanism transforms the model parameters of WFL from standard floating-point representations, necessitating error-free transmissions, into a new fixed-point format that only requires the fraction bits to be transmitted, tolerates bit errors in the model parameters received, and can thus “enjoy” communication noise for privacy protection.

The contributions of this paper are summarized as follows.

- We propose a novel mechanism to protect the privacy of WFL by leveraging inherently noisy wireless channels. The mechanism obfuscates model parameters in bits, compatible with floating-point standards, *e.g.*, IEEE 754, widely adopted in the systems.
- We design a novel floating-point-to-fixed-point conversion that not only significantly reduces the number of transmitted bits but, more importantly, eliminates the risk of catastrophic model distortion associated with transmissions and noise corruption of the sign or exponent bits of floating-point model parameters.
- We prove that the proposed mechanism strictly satisfies (λ, ϵ) -Rényi DP. This involves the analysis of a new metric to measure the bit-level distance, concerning bitstreams encoded from local model parameters, and rigorous derivation of the bit-flipping probability.
- We analytically corroborate the convergence of WFL under the proposed mechanism, revealing that the convergence upper bound is affected not only by the privacy

Table I: Notation and definitions

Notation	Definition
n, N	Device index, and total number of devices
\mathcal{N}	Set of device indices
m, M	Dimension index, and total number of model dimensions
j	Bit index in the fraction part
K	Total number of communication rounds
E	Total number of local training iterations per round
\mathcal{I}_E	Index set of iterations that collects global aggregations
t, T	Index and total number of local training iterations
d, \mathcal{D}	Data point, and dataset
$\mathbf{w}_{t,n}$	Input model of device n at the t -th iteration
$\boldsymbol{\omega}_{t,n}$	Output model of device n at the t -th iteration
$\tilde{\boldsymbol{\omega}}$	Recovered local model (with error) at server
$\tilde{\mathbf{u}}$	Bitstream perturbed by artificial noise
$\hat{\mathbf{u}}$	Bitstream perturbed by artificial and communication noise
$\boldsymbol{\omega}_{t,\mathcal{G}}$	Global model at the t -th local training iteration
$\Delta\omega_{\max}$	Classical sensitivity
$\bar{\kappa}_{\Delta\omega_{\max}}$	Expected bit-level distance
ν_2, ν_∞	Maxima of the ℓ_2 -norm and ℓ_∞ -norm of the model parameter vector

budget but also by the number of total training iterations and local epochs per communication round.

Extensive experiments validate the privacy and convergence analysis of the proposed channel-native bit-flipping DP mechanism for WFL. Two image classification tasks are performed, using a convolutional neural network (CNN) on the Federated Extended MNIST (F-MNIST) dataset and using the 18-layer residual network (ResNet-18) on the Federated CIFAR100 (Fed-CIFAR100) dataset. Our mechanism markedly outperforms its channel-agnostic counterparts, and exhibits substantial superiority to the state-of-the-art Gaussian mechanism developed under the prerequisite that only the error-free parts of (obfuscated) local model parameters are aggregated.

The rest of this paper is organized as follows. The related works are discussed in Section II, followed by the system model in Section III. In Section IV, we present the new channel-native bit-flipping DP mechanism. The privacy and convergence of WFL under the mechanism are discussed in Sections V and VI, respectively. Experiments are presented in Section VII, followed by conclusions in Section VIII. Table I collates the notation used in this paper.

II. RELATED WORK

This section summarizes the studies on privacy preservation in FL/WFL systems. Although many have been on the privacy of WFL, none have perturbed WFL model parameters at the bit level nor considered practical floating-point data formats used in digital systems.

A. Privacy-Preserving FL/WFL

Existing studies have mainly focused on perturbing the model parameters in decimal amplitude prior to digitization to bitstreams, as depicted in Fig. 1(a). In [14] and [15], artificial Gaussian noise was applied to the (decimal) local model parameters before model transmission and aggregation, where

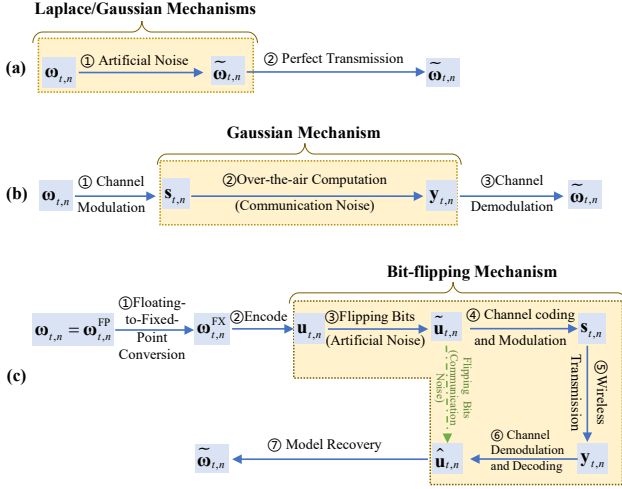


Fig. 1. The workflows of the local model transmission of device n under different DP mechanisms when $t \in \mathcal{I}_E$: (a) Channel-agnostic DP mechanisms, *e.g.*, Laplace or Gaussian mechanism, only use artificial noise and do not exploit noisy communication channels; (b) The DP mechanism for OTA-FL systems uses the additive Gaussian noise to protect privacy, but does not support digital transmission; (c) The proposed channel-native bit-flipping DP mechanism.

the DP requirement was satisfied by adapting the variance of the Gaussian noise. The authors of [10] and [15] demonstrated analytically and experimentally that the DP-based FL/WFL with the Laplace mechanism is worse than that with the Gaussian mechanism because the Laplacian mechanism adds larger noises sampled from a Laplacian distribution, which is farther away from its mean. Yuan *et al.* [15] designed a novel amplitude-varying perturbation mechanism, where the DP noise is a geometric series changing over global aggregations to balance the privacy and utility in FL/WFL. All these schemes perturb the model parameters of FL/WFL in the decimal domain before the model parameters are digitized into bitstreams, yielding floating-point number structures.

B. WFL under Imperfect Communications

Many studies have attempted to develop communication-efficient algorithms to improve the performance of WFL, without consideration of the privacy of model parameters. Model compression [17], [22] and quantization [23] have been exploited to reduce communication overhead, at the cost of FL performance due to compression and quantization errors. In [18], it was revealed that the user transmission success probability, affected by unreliable and resource-constrained wireless channels, critically affects the convergence of WFL. In [24], a user datagram protocol with retransmissions was employed to recover from model transmission failures at the cost of delays and signaling overhead. Operating in the analog domain, OTA-FL allows the participating clients to upload their models within the same resource block [17], [25], [26]. These models can be aggregated over the air due to the additivity of signals in the electromagnetic field. OTA-FL suffers from imperfect channel state information (CSI) with estimation errors [27]. No consideration has been given to the privacy of the model parameters in these studies.

C. Privacy-Preserving WFL

Some studies [13], [19], [28] have started to utilize the system-level noises, *e.g.*, quantization errors or communication noise, to implement DP mechanisms. None is applicable to digital communication systems that have the potential to enjoy privacy protection offered by noisy wireless channels. In [28], devices quantize and compress their local model parameters with a required bit rate, resulting in a quantization error that helps the system to satisfy a predefined privacy level. However, the privacy-preserving capability of noisy communication channels was overlooked. In the context of OTA-FL, Liu *et al.* [13] exploited the additive Gaussian communication noise to perform the analog waveforms modulated from uncoded model parameters as a privacy-preserving mechanism, and the transmit power was dynamically controlled to satisfy the privacy requirement, as illustrated in Fig. 1(b). In [19], the use of Gaussian communication and artificial noises was extended to decentralized OTA-FL systems. A prescribed privacy requirement was proven in peer-to-peer communication. However, both of the studies [13], [19] relied on the prerequisite of OTA-FL, only applicable to Gaussian noises in the analog signal domain, and cannot be extended to digital systems.

III. PRELIMINARIES AND SYSTEM MODEL

In this section, we provide the preliminaries of the WFL model, (λ, ϵ) -Rényi DP, and floating-point number structure, and the considered threat model in the context of WFL.

A. WFL Model

Consider a WFL system with a central server (*e.g.*, access point or AP) and N devices. $\mathcal{N} = \{1, \dots, N\}$ collects the indexes of the devices. Device $n \in \mathcal{N}$ owns a dataset \mathcal{D}_n with $|\mathcal{D}_n|$ data samples. The local loss function of device n is

$$F_n(\mathbf{w}, \mathcal{D}_n) = \frac{1}{|\mathcal{D}_n|} \sum_{d \in \mathcal{D}_n} f(d, \mathbf{w}), \quad (1)$$

where $\mathbf{w} \in \mathbb{R}^{M \times 1}$ is an M -dimensional model parameter vector, $d \in \mathcal{D}_n$ is the data sample, and $f(d, \mathbf{w})$ is the loss function concerning d and \mathbf{w} .

The objective of the WFL system is to find the optimal model parameter vector $\mathbf{w}^* = \arg \min_{\mathbf{w} \in \mathbb{R}^{M \times 1}} F(\mathbf{w})$, where $F(\mathbf{w})$ being the global loss function which is the weighted sum of the local loss functions of all devices, as given by

$$F(\mathbf{w}) = \sum_{n \in \mathcal{N}} q_n F_n(\mathbf{w}, \mathcal{D}_n), \quad (2)$$

where $q_n = \frac{|\mathcal{D}_n|}{\sum_{n \in \mathcal{N}} |\mathcal{D}_n|}$ is the coefficient of device n . Let F_n^* and F^* denote the minima of $F_n(\mathbf{w})$ and $F(\mathbf{w})$, respectively.

The WFL training consists of training iterations, with adequate synchronization across all devices. Let K denote the total number of communication rounds for each device, and E denote the number of local training iterations per communication round. The training process has a total of $T = KE$ local training iterations. Let $\mathcal{I}_E = \{0, E, 2E, \dots, KE\}$ collect the iterations when global aggregations take place.

At the beginning of the k -th communication round, the server broadcasts the latest global model to all clients. Each

device n trains its local model for E local iterations based on the global model and its local data \mathcal{D}_n . The local models of the devices, $\omega_{t,n}, \forall n$, are updated in parallel when $t \notin \mathcal{I}_E$.

When $t \in \mathcal{I}_E$, the devices first update their local models $\omega_{t,n}, \forall n$, then randomly flips the fraction bits of its m -th element, *i.e.*, $\omega_{t,n,m} \in \omega_{t,n}$ with $m = 1, \dots, M$, to perturb $\omega_{t,n}$ and uploads the perturbed local models through a noisy channel to the server. The server aggregates the received local models, *i.e.*, $\tilde{\omega}_{t,n}, \forall n$, to update the global model, $\omega_{t,G} = \sum_{n \in \mathcal{N}} q_n \tilde{\omega}_{t,n}$, and broadcasts $\omega_{t,G}$ to all devices for further updating their local models.

Suppose full-batch gradient descent over training iterations, $\forall t = 1, 2, \dots, T$. The local model of device n at the $(t+1)$ -th (local) iteration is updated as

$$\omega_{t+1,n} = \mathbf{w}_{t,n} - \eta \cdot \text{Clip}_G(\nabla F_n(\mathbf{w}_{t,n}, \mathcal{D}_n)), \quad \forall t, n, \quad (3)$$

where

$$\mathbf{w}_{t,n} = \begin{cases} \omega_{t,n}, & \text{if } t \notin \mathcal{I}_E; \\ \omega_{t,G} = \sum_{n \in \mathcal{N}} q_n \tilde{\omega}_{t,n}, & \text{if } t \in \mathcal{I}_E, \end{cases} \quad (4)$$

is the input of the $(t+1)$ -th (local) iteration, and $\omega_{t+1,n}$ is the corresponding output of the local training. Moreover, η is the learning rate, $\nabla F_n(\cdot)$ denotes the gradient of $F_n(\cdot)$, $\text{Clip}_G(\nabla F_n(\mathbf{w}, \mathcal{D}_n)) = \frac{1}{|\mathcal{D}_n|} \sum_{d \in \mathcal{D}_n} \nabla f(d, \mathbf{w}) \cdot \min\{1, \frac{G}{\|\nabla f(d, \mathbf{w})\|_2}\}$ is the clipped operator with the gradient clipping threshold G^1 .

Next, we pre-train the model and record the maxima of the ℓ_2 -norm and ℓ_∞ -norm of the model parameter vector, denoted by $\nu_2 = \max_{\forall t,n} \|\omega_{t,n}\|_2$ and $\nu_\infty = \max_{\forall t,n} \|\omega_{t,n}\|_\infty$, respectively, both of which increase with G .

B. Threat Model

A critical risk arises from within the WFL system due to an honest but curious server. The server can legally access the local models trained by the devices, infer their training data, and compromise their privacy; *i.e.*, launching an inference attack [30]. This happens when the server has overlapping datasets with the devices and can analyze their local training inputs and outputs to infer their local data.

Encryption cannot stop the server from launching inference attacks on the local models, but it can prevent outsiders from accessing the local models. As a matter of fact, the transmissions between the devices and the server are typically encrypted. Computationally efficient symmetric encryption, such as Advanced Encryption Standard (AES) [31] and Data Encryption Standard (DES) [32], can be reasonably employed to secure the model transmissions. While homomorphic encryption can prevent the server from deciphering the local models, it requires all devices to use the same private key and cannot stop them from eavesdropping on each other. Moreover, homomorphic encryption is typically computationally expensive and needs a trusted third party for key agreement [33].

¹We adopt gradient clipping to ensure stable training and compatibility with practical ML algorithms. Gradient clipping has been extensively adopted in ML (with or without DP) to mitigate gradient explosion and preserve convergence; see [29] and references therein.

To this end, it is reasonable to consider the threat imposed by an honest but curious server. For illustration convenience, we assume the uploaded local models are not encrypted when elaborating on the proposed channel-native bit-flipping DP mechanism. Then, we show that the mechanism can apply when the local models are encrypted with symmetric keys.

C. (λ, ϵ) -Rényi DP

In this paper, we consider the Rényi DP mechanism to protect the privacy of the devices. The definition of (λ, ϵ) -Rényi DP is provided as follows.

Definition 1 ((λ, ϵ) -Rényi DP [8]). *The randomized mechanism $\mathcal{M} : \mathcal{D} \mapsto \mathbb{R}$ satisfies ϵ -Rényi DP of order λ , (λ, ϵ) -Rényi, if, for any adjacent datasets \mathcal{D} and \mathcal{D}' , it holds that*

$$D_\lambda(\mathcal{M}(\mathcal{D}) \parallel \mathcal{M}(\mathcal{D}')) \leq \epsilon,$$

where the Rényi divergence of order $\lambda > 1$ is defined as

$$D_\lambda(\mathcal{M}(\mathcal{D}) \parallel \mathcal{M}(\mathcal{D}')) \triangleq \frac{1}{\lambda-1} \ln \left[\mathbb{E}_{x \sim \mathcal{M}(\mathcal{D}')} \left(\frac{\mathcal{M}(\mathcal{D})}{\mathcal{M}(\mathcal{D}')} \right)^\lambda \right].$$

Note that the Rényi divergence recedes to the Kullback-Leibler divergence, *i.e.*, $D_1(\mathcal{M}(\mathcal{D}) \parallel \mathcal{M}(\mathcal{D}')) = D_{\text{KL}}(\mathcal{M}(\mathcal{D}) \parallel \mathcal{M}(\mathcal{D}'))$, when $\lambda = 1$.

D. Floating-Point Number Format

For illustration, we consider the single-precision floating-point format², **binary32**, which is the most commonly used computer number representation that typically requires 32 bits of memory, and follows the IEEE 754 standard [21]. A **binary32** number comprises a sign bit, 8 exponent bits, and 23 fraction bits with an additional, implicit leading “1” bit to the left of the binary point [21]. The (decimal) value of a **binary32** number, $a = (a_{31}a_{30} \dots a_0)_2$, is³

$$\begin{aligned} a &= (-1)^{a_{31}} \times 2^{(a_{30}a_{29} \dots a_{23})_2 - 127} \times (1.a_{22} \dots a_0)_2 \\ &= (-1)^{a_{31}} \times 2^{(a_{30}a_{29} \dots a_{23})_2 - 127} \times \left(1 + \sum_{i=1}^{23} a_{23-i} 2^{-i} \right). \end{aligned}$$

When the bits in the fraction part of a **binary32** floating-point number are randomly flipped with probability p , the mean and expectation of the resulting floating-point number in decimal are provided in the following lemma.

Lemma 1. *For a **binary32** number $a = (a_{31}a_{30} \dots a_0)_2$, after flipping its bits with a probability of p in the fraction part, the mean of the output \tilde{a} in decimal is given by*

$$\mathbb{E}(\tilde{a}) = (1-2p)a + (-1)^{a_{31}} 2^{(a_{30}a_{29} \dots a_{23})_2 - 127} \left(2p + \sum_{i=1}^{23} 2^{-i} p \right), \quad (5)$$

and the variance of \tilde{a} is given by

$$\text{Var}(\tilde{a}) = \frac{(1-4^{-23})}{3} p(1-p) \left(2^{2(a_{30}a_{29} \dots a_{23})_2 - 254} \right). \quad (6)$$

Proof. See **Appendix A**. \square

²IEEE 754 also defines other binary floating-point formats, *e.g.*, half-precision, double-precision, quadruple-precision, and octuple-precision. The proposed analysis and algorithm are applicable to all these formats.

³The implicit “1” bit before the fractional bits is not explicitly stored in the memory to save space and remains “1” for normalized numbers [21].

IV. CHANNEL-NATIVE PRIVACY PROTECTION FOR WFL

In this section, we delineate the new *channel-native bit-flipping DP mechanism*. Considering numerical data is stored and transmitted in bits, *e.g.*, using the **binary32** floating-point format, and noisy wireless channels cause bit errors, we protect the privacy of the model parameters by having their bits randomly flipped by the clients and noisy wireless channels.

The new mechanism involves a new method for converting floating-point model parameters to fixed-point counterparts so that only the bits accounting for the fraction part of the model parameters can be meaningfully perturbed (as flipping the sign or exponent bits could dramatically distort the model parameters). The mechanism also involves a new way to evaluate the sensitivity regarding the number of different bits between fixed-point model parameters.

A. Proposed Floating-Point-to-Fixed-Point Conversion

When $t \in \mathcal{I}_E$, each element of $\omega_{t,n}$ is bounded by the ℓ_∞ -norm of $\omega_{t,n}$, *i.e.*, $|\omega_{t,n,m}| \leq \nu_\infty$, where $\omega_{t,n,m}$ is the m -th element of $\omega_{t,n}$ with $m = 1, \dots, M$. The ℓ_∞ -norm, ν_∞ , is expressed in the **binary32** format as $\nu_\infty = (-1)^{c_{31}} \times 2^{(c_{30}c_{29}\dots c_{23})_2 - 127} \times \left(1 + \sum_{i=1}^{23} 1 \cdot c_{23-i} \cdot 2^{-i}\right)$. Since $\nu_\infty \geq |\omega_{t,n,m}| \geq 0$ is positive, the sign bit c_{31} is set to 0. The upper bound of ν_∞ is achieved when $c_{22}c_{21}\dots c_0 = 11\dots 1$, resulting in $1 + \sum_{i=1}^{23} 2^{-i} = 2 - 2^{-23} \leq 2$. By contrast, the lower bound is achieved when $c_{22}c_{21}\dots c_0 = 00\dots 0$, yielding $1 + \sum_{i=1}^{23} 0 \cdot 2^{-i} = 1$. Consequently, ν_∞ is bounded as $2^{(c_{30}c_{29}\dots c_{23})_2 - 127} \leq \nu_\infty \leq 2^{(c_{30}c_{29}\dots c_{23})_2 - 126}$. After clipping, the model parameter $\omega_{t,n}$ is restricted to the range $[-2^{(c_{30}c_{29}\dots c_{23})_2 - 126}, 2^{(c_{30}c_{29}\dots c_{23})_2 - 126}]^{M \times 1}$.

A critical and novel step of the proposed approach is converting $\omega_{t,n} \triangleq \omega_{t,n}^{\text{FP}}$ from a floating-point number into a fixed-point number $\omega_{t,n}^{\text{FX}}$ by adding a constant to each model element $\omega_{t,n,m}$, $\forall m$ of $\omega_{t,n}^{\text{FP}}$. The constant is $3 \times 2^{(c_{30}c_{29}\dots c_{23})_2 - 126}$, determined by the exponent part of the floating-point number ν_∞ , *i.e.*, $(c_{30}c_{29}\dots c_{23})_2$. Adding this constant to every element of $\omega_{t,n}^{\text{FP}}$ converts $\omega_{t,n}^{\text{FP}}$ from a **binary32** floating-point number to a fixed-point number within the following range:

$$\omega_{t,n}^{\text{FX}} \triangleq \omega_{t,n}^{\text{FP}} + \{3 \times 2^{(c_{30}c_{29}\dots c_{23})_2 - 126}\}^{M \times 1} \in [2^{(c_{30}c_{29}\dots c_{23})_2 - 125}, 2^{(c_{30}c_{29}\dots c_{23})_2 - 124}]^{M \times 1}. \quad (7)$$

By this means, all elements of $\omega_{t,n}^{\text{FX}}$, $\forall n, t$ share the same positive (+) sign and exponent values of $(c_{30}c_{29}\dots c_{23})_2 + 2$.

The proposed floating-point-to-fixed-point conversion eliminates the need to transmit the sign and exponent bits of the original floating-point number, *i.e.*, $c_{31}c_{30}\dots c_{23}$, since those bits are converted to $(c_{30}c_{29}\dots c_{23})_2 + 2$ with $c_{31} = 0$, which are consistent across all devices and known to the server (as $c_{30}c_{29}\dots c_{23}$ depends only on the common ν_∞). To obtain the public ν_∞ , the server can pre-train the FL model using publicly available datasets, compute the ℓ_∞ -norm (denoted as ν_∞), and then broadcast this public information to all clients. Each client can also pre-train its model locally and compute its own ℓ_∞ -norm. If the public ℓ_∞ -norm is larger than the client's local ℓ_∞ -norm, the client decides to participate in the FL task. In other words, ν_∞ is publicly shared and does not leak

privacy. More importantly, withholding the sign and exponent bits prevents the sign and exponent bits of the floating-point model parameters from being flipped at the devices and during transmissions through noisy wireless channels, as flipping those bits could drastically distort the model parameters.

As a result of the floating-point-to-fixed-point conversion, each device n only needs to encode the fraction part of the fixed-point model parameter $\omega_{t,n}^{\text{FX}}$ into a bitstream, denoted by $\mathbf{u}_{t,n} \in \mathbb{B}^{23M \times 1}$, where $\mathbb{B} = \{0, 1\}$ is the set of binary numbers. The number of bits to be transmitted is $23M$ per local model; cf. $32M$ under **binary32**.

B. Bit Flipping and Model Transmission

Two types of noises are experienced when the fixed-point bitstream of a local model, $\mathbf{u}_{t,n} \in \mathbb{B}^{23M \times 1}$, is uploaded from a device n to the server: The artificial bit-flipping noise imposed by the clients, and the inherent communication noise. Both artificial and communication noises are imposed into the bitstreams, $\mathbf{u}_{t,n}$, $\forall n$, that are generated from the fraction parts of the transformed fixed-point model parameters. The floating-point-to-fixed-point conversion eliminates the need to transmit the sign and exponent bits of the floating-point numbers, ensuring those bits are unaffected by communication noise.

1) *Artificial Noise*: Each device n perturbs the bitstream $\mathbf{u}_{t,n}$ by flipping the bits at random with a pre-defined bit-flipping probability, denoted by $p_{t,n,A}$. The resulting flipped bitstream is denoted as

$$\tilde{\mathbf{u}}_{t,n} = \mathbf{u}_{t,n} \otimes \mathbf{e}_{t,n,A}, \quad \mathbf{e}_{t,n,A} \sim \mathcal{B}(23M, 1 - p_{t,n,A}), \quad (8)$$

where $\mathcal{B}(23M, 1 - p)$ is the binomial distribution with length $23M$ and probability $(1 - p)$; and \otimes is the element-wise exclusive-NOR operator. Device n encodes and modulates $\tilde{\mathbf{u}}_{t,n}$ into $\mathbf{s}_{t,n}$, which is a sequence of symbols to be transmitted to the server. The length of $\mathbf{s}_{t,n}$ depends on the modulation-and-coding scheme employed, more specifically, the transmit rate of the scheme, *e.g.*, rM for r - γ QAM with r being the coding rate and γ being the modulation order of QAM/QPSK signals⁴. $\mathbf{s}_{t,n} \in \mathbb{R}^{\frac{23M}{r\gamma} \times 1}$.

2) *Communication Noise*: Suppose the wireless channels experience block fading; *i.e.*, the channel coefficients remain constant during a round but may vary independently between rounds. The system bandwidth is B_n (in Hz) in the t -th communication round. Consider a baseline setting with a single-antenna server and single-antenna devices. At the server, the received sequence of symbols from device n in the t -th communication round can be modeled as:

$$\mathbf{y}_{t,n} = h_{t,n} \sqrt{\beta_{t,n}} \mathbf{s}_{t,n} + \boldsymbol{\theta}_{t,n},$$

where $h_{t,n}$ is the complex-valued channel coefficient for device n in the t -th communication round, $\beta_{t,n}$ denotes the transmit power of device n during the t -th round, and $\boldsymbol{\theta}_{t,n} \in \mathbb{R}^{\frac{23M}{r\gamma} \times 1}$ is the communication noise undergone at the server (or AP), with power spectral density N_0 (Watts/Hz).

On receiving $\mathbf{y}_{t,n}$, the server decodes and demodulates the signal to recover the transmitted signal sequence $\mathbf{s}_{t,n}$. The

⁴Channel coding is typically used to combat fading and noise. It is optional here as it weakens the privacy-preserving capability of wireless channels.

demodulation process converts the received signal sequence into a bitstream, denoted by $\hat{\mathbf{u}}_{t,n} \in \mathbb{B}^{23M \times 1}$. Bit errors can occur due to communication noises and channel impairments. $\tilde{\mathbf{u}}_{t,n}$ and $\hat{\mathbf{u}}_{t,n}$ likely differ.

The BER, denoted by $p_{t,n,C}$, can be obtained based on the prior knowledge of the channel parameters, *e.g.*, $h_{t,n}, \beta_{t,n}, N_0$ and B_n , as well as the coding-and-modulation schemes (*e.g.*, BPSK, QPSK, *etc.*) and channel conditions (*e.g.*, AWGN, Rayleigh fading, *etc.*) [34]. Taking BPSK and QPSK over AWGN channel as an example, the signal-to-noise ratio (SNR) is $\gamma_{t,n} = \frac{(h_{t,n})^2 \beta_{t,n}}{N_0 B_n}$, and the communication BER is $p_{t,n,C} = Q(\sqrt{2\gamma_{t,n}})$ [35], where $Q(x) = \frac{1}{\sqrt{2\pi}} \int_x^\infty e^{-\frac{x^2}{2}} dx$ is the error function [34]. Note that our analysis of the proposed mechanism is not limited to a specific channel model.

As a result, the received bitstream is denoted by

$$\hat{\mathbf{u}}_{t,n} = \tilde{\mathbf{u}}_{t,n} \otimes \mathbf{e}_{t,n,C}, \quad \mathbf{e}_{t,n,C} \sim \mathcal{B}(23M, 1 - p_{t,n,C}). \quad (9)$$

3) *End-to-End Bit Error*: From $\mathbf{u}_{t,n}$ to $\hat{\mathbf{u}}_{t,n}$, a bit may flip up to twice due to the artificial bit-flipping noise and communication noise. A bit is erroneous if flipped once. As a result, the end-to-end BER, denoted by $p_{t,n}$, is given by

$$\begin{aligned} p_{t,n} &= p_{t,n,C}(1 - p_{t,n,A}) + p_{t,n,A}(1 - p_{t,n,C}) \\ &= p_{t,n,C} + p_{t,n,A} - 2p_{t,n,C}p_{t,n,A}. \end{aligned} \quad (10)$$

The BER from the artificial bit-flipping noise, $p_{t,n,A}$, is

$$p_{t,n,A} = \frac{p_{t,n} - p_{t,n,C}}{1 - 2p_{t,n,C}}. \quad (11)$$

Note that the required end-to-end BER, $p_{t,n}$, corresponds to the privacy requirement specified by the privacy budget of the devices. With a given modulation-and-coding scheme and channel condition, the BER stemming from the wireless transmissions of the local models, *i.e.*, $p_{t,n,C}$, can be measured through the reciprocity of wireless channels. Given $p_{t,n}$ and $p_{t,n,C}$, $p_{t,n,A}$ can be accordingly specified.

We now formalize the proposed bit-flipping mechanism with respect to the end-to-end bit-flipping probability (or, in other words, end-to-end BER), p , as follows.

Definition 2 (Bit-flipping DP Mechanism). *For a local dataset \mathcal{D} and an encoded bit stream of a model parameter, *i.e.*, $\mathbf{u}(\cdot) \in \mathbb{B}^{23M \times 1}$, the randomized bit-flipping DP mechanism is defined as*

$$\mathcal{M}_{\text{BF}}(\mathcal{D}, \mathbf{u}(\cdot), \bar{\kappa}_{\Delta\omega_{\max,n}}, \lambda, \epsilon) = \mathbf{u}(\mathcal{D}) \otimes \mathcal{B}(23M, 1 - p), \quad (12)$$

where $\mathcal{B}(23M, 1 - p)$ is the binomial distribution with length $23M$ and probability $(1 - p)$; $\bar{\kappa}_{\Delta\omega_{\max,n}}$ is the expected bit-level distance under a given classical sensitivity $\Delta\omega_{\max,n}$; \otimes is the element-wise exclusive-NOR (XNOR) operator.

C. Model Recovery

With the prior knowledge about the sign and exponent parts of the fixed-pointed numbers, the server can first recover the local models after demodulating and decoding the bitstream $\hat{\mathbf{u}}_{t,n}$. This is done by concatenating the sign and exponent parts of the fixed-point number to $\hat{\mathbf{u}}_{t,n}$, followed by subtracting

$3 \times 2^{(c_{30}c_{29} \cdots c_{23})_2 - 126}$ from the decimal fixed-point elements to recover the floating-point local models. The recovered local model parameters of device n are denoted by $\tilde{\omega}_{t,n}$.

D. Implementation Details

Algorithm 1 summarizes the proposed channel-native bit-flipping DP mechanism. Specifically, after finishing the local training in Line 6, the encoding process starts. As described in Lines 7 to 12, at the beginning of the encoding process, the clients convert the **binary32** floating-point model parameters $\omega_{t,n}$ to fixed-point numbers by adding a constant generated from $\nu_\infty = (c_{31}c_{30} \cdots c_0)_2$; see (7). Then, the clients remove the common sign part (*i.e.*, 1) and exponent part (*i.e.*, $(c_{30}c_{29} \cdots c_{23})_2 + 2$) of the fixed-point numbers, and encode the fraction part into a bitstream $\mathbf{u}_{t,n}$ (see Section IV-A). The clients also estimate the BERs $p_{t,n,A}$; see Line 13. Based on the BERs and privacy requirements, the clients calculate the artificial bit-flipping probabilities needed to supplement the inherent privacy provided by the channels; see (11).

Then, artificial and communication bit-flipping operations, performed by the clients and caused by the noisy channels, are sequentially added to the bitstream to enhance privacy. The former is done according to (8) before transmission; see Line 14. The latter comes from the noisy communication channel according to (9); see Line 15. After receiving all bitstreams $\{\hat{\mathbf{u}}_{t,n}, \forall t, n\}$ from the clients, the server reconstructs the fixed-point numbers with the common sign and exponent parts (*i.e.*, 1 and $(c_{30}c_{29} \cdots c_{23})_2 + 2$), and subtracts the common value to recover the original **binary32** model parameters $\tilde{\omega}_{t,n}$ (see Sec. IV-C), as shown in Line 18. The received models are aggregated at the server using (4) in Line 19.

V. PRIVACY ANALYSIS

Our approach adapts standard privacy analysis to operate at the bit level. Specifically, the sensitivity of the model parameters, $\Delta\omega_{\max}$, is first evaluated, as in conventional DP algorithms. Then, the bit-level distances between parameter pairs achieving $\Delta\omega_{\max}$ are analyzed statistically. Finally, the Renyi divergence is analyzed based on these binary distances instead of the original parameter values. This adaptation ensures privacy guarantees are upheld while capturing the nuances of parameter representation at the bit level.

A. Bit-Level Distance

When $t \in \mathcal{I}_E$, a certain level of superimposed artificial noise and communication noise, resulting in the end-to-end BER $p_{t,n}$, is imposed to the model parameter $\omega_{t,n}(\mathcal{D}_n)$ of every device n . This results in a perturbed model parameter $\tilde{\omega}_{t,n}(\mathcal{D}_n) = \omega_{t,n}(\mathcal{D}_n) + \mathbf{z}_{t,n}$ at the server.

Suppose that $\omega_{t,n}(\mathcal{D}_n)$ and $\omega_{t,n}(\mathcal{D}'_n)$ are derived from two adjacent datasets \mathcal{D}_n and $\mathcal{D}'_n = \mathcal{D}_n \cup \{d'\}$, respectively. d' is a data sample. To measure the sensitivity between these two sets of model parameters, we use the ℓ_2 -norm. The (classical) sensitivity concerning function $\omega_{t,n}(\mathcal{D}_n)$ is given by

$$\Delta\omega_{\max,n} = \max_{\forall t, \mathcal{D}_n, \mathcal{D}'_n} \|\omega_{t,n}(\mathcal{D}_n) - \omega_{t,n}(\mathcal{D}'_n)\|_2 = \frac{2\eta G}{|\mathcal{D}_n|}, \quad (13)$$

Algorithm 1 Channel-native bit-flipping DP mechanism

Initialization: Clipping threshold G ; maxima of ℓ_∞ -norm ν_∞ ; initial global model $\omega_{0,G}$; number of local epochs E ; total number of training iterations T .

```

1: for  $t = 1, \dots, T$  do
2:   for all devices  $n \in \mathcal{N}$  in parallel do
3:     if  $t \notin \mathcal{I}_E$  then
4:       Perform local training with (3) and obtain  $\omega_{t,n}$ ;
5:     else
6:       Perform local training with (3) and obtain  $\omega_{t,n}$ ;
7:       Encode a local model  $\omega_{t,n}$  into a bitstream  $\mathbf{u}_{t,n}$ ,
         as follows:
8:       Initialize:  $\omega_{t,n}^{\text{FP}} = \omega_{t,n}$ ,  $\nu_\infty$ ;
9:       Obtain the binary format of  $\nu_\infty = (c_{31}c_{30}\dots c_0)_2$ ;
10:      Perform floating-point-to-fixed-point conversion with (7)
         and obtain  $\omega_{t,n}^{\text{FX}}$ ;
11:      Remove the common sign and exponent parts of  $\omega_{t,n}^{\text{FX}}$ ,
         i.e., 1 and  $(c_{30}c_{29}\dots c_{23})_2 + 2$ ;
12:      Encode the fraction part of  $\omega_{t,n}^{\text{FX}}$  and obtain  $\mathbf{u}_{t,n}$ ;
13:      Calculate the artificial BER  $p_{t,n,A}$ ;
14:      Add artificial bit-flipping noise to the bitstream
          $\mathbf{u}_{t,n}$  to obtain  $\tilde{\mathbf{u}}_{t,n}$ , see (8);
15:      Modulate and upload  $\tilde{\mathbf{u}}_{t,n}$  to the server through
         the noisy wireless channel, see (9);
16:     end if
17:   end for
18:   The server receives signals from all devices, obtains
      $\hat{\mathbf{u}}_{t,n}$ , and recovers  $\tilde{\omega}_{t,n}$ .
19:   The server aggregates all local models and obtains  $\omega_{t,G}$ ,
     see (4).
20: end for

```

which is obtained from

$$\begin{aligned} & \|\omega_{t,n}(\mathcal{D}_n) - \omega_{t,n}(\mathcal{D}'_n)\|_2 \\ &= \left\| \left(\frac{\eta}{|\mathcal{D}_n|} - \frac{\eta}{|\mathcal{D}'_n|} \right) \sum_{d \in \mathcal{D}_n} \nabla f(d, \mathbf{w}) \cdot \min \left\{ 1, \frac{G}{\|\nabla f(d, \mathbf{w})\|_2} \right\} \right. \\ & \quad \left. - \frac{\eta}{|\mathcal{D}'_n|} \nabla f(d', \mathbf{w}) \cdot \min \left\{ 1, \frac{G}{\|\nabla f(d', \mathbf{w})\|_2} \right\} \right\|_2 \end{aligned} \quad (14a)$$

$$\begin{aligned} & \leq \left\| \frac{\eta}{|\mathcal{D}_n|(|\mathcal{D}_n|+1)} \sum_{d \in \mathcal{D}_n} \nabla f(d, \mathbf{w}) \cdot \min \left\{ 1, \frac{G}{\|\nabla f(d, \mathbf{w})\|_2} \right\} \right\|_2 \\ & \quad + \left\| \frac{\eta}{|\mathcal{D}'_n|+1} \nabla f(d', \mathbf{w}) \cdot \min \left\{ 1, \frac{G}{\|\nabla f(d', \mathbf{w})\|_2} \right\} \right\|_2 \end{aligned} \quad (14b)$$

$$\begin{aligned} & \leq \frac{\eta}{|\mathcal{D}_n|(|\mathcal{D}_n|+1)} \sum_{d \in \mathcal{D}_n} \left\| \nabla f(d, \mathbf{w}) \cdot \min \left\{ 1, \frac{G}{\|\nabla f(d, \mathbf{w})\|_2} \right\} \right\|_2 \\ & \quad + \frac{\eta}{|\mathcal{D}'_n|+1} \left\| \nabla f(d', \mathbf{w}) \cdot \min \left\{ 1, \frac{G}{\|\nabla f(d', \mathbf{w})\|_2} \right\} \right\|_2 \end{aligned} \quad (14c)$$

$$\leq \frac{2\eta G}{|\mathcal{D}'_n|}, \quad (14d)$$

where (14a) is based on (3) and reorganization, (14b) is due to the homogeneity of ℓ_2 -norm and that $|\mathcal{D}'_n| = |\mathcal{D}_n| + 1$, (14c) is due to the homogeneity of ℓ_2 -norm, and (14d) is based on $\frac{1}{|\mathcal{D}_n|+1} \leq \frac{1}{|\mathcal{D}_n|}$ and $\left\| \nabla f(d, \mathbf{w}) \cdot \min \left\{ 1, \frac{G}{\|\nabla f(d, \mathbf{w})\|_2} \right\} \right\|_2 \leq G$.

1) *Definition of Expected Bit-Level Distance:* Since we consider perturbation upon the bitstreams $\mathbf{u}_{t,n}$ (through artificial bit-flipping and communication noises), which is also a function of \mathcal{D}_n , i.e., $\mathbf{u}_{t,n} = \mathbf{u}_{t,n}(\mathcal{D}_n)$, we are interested in the difference between the pair of bitstreams corresponding to $\Delta\omega_{\max,n}$ before the perturbation. It is important to note that

the difference is non-deterministic and influenced by various sources of inherent randomness, including dropout mechanisms in the CNN model, random seeds, and the stochastic padding algorithm defined in the IEEE 754 standard. We amount to the expectation of the bit-level difference corresponding to $\Delta\omega_{\max,n}$ and accordingly define a new metric, which will be employed in the privacy analysis of the proposed mechanism in Section V-B.

Consider two bitstreams $\mathbf{u}_{t,n}(\mathcal{D}_n)$ and $\mathbf{u}_{t,n}(\mathcal{D}'_n)$, each derived from the respective model parameters, $\omega_{t,n}(\mathcal{D}_n)$ and $\omega_{t,n}(\mathcal{D}'_n)$, with their difference equal to the classical sensitivity, $\Delta\omega_{\max,n} \equiv \|\omega_{t,n}(\mathcal{D}_n) - \omega_{t,n}(\mathcal{D}'_n)\|_2$. The bit-level distance between $\mathbf{u}_{t,n} \triangleq \mathbf{u}_{t,n}(\mathcal{D})$ and $\mathbf{u}'_{t,n} \triangleq \mathbf{u}_{t,n}(\mathcal{D}')$ is defined by

$$\begin{aligned} \kappa(\omega_{t,n}(\mathcal{D}_n), \omega_{t,n}(\mathcal{D}'_n)) & \triangleq \|\mathbf{u}_{t,n}(\mathcal{D}_n) - \mathbf{u}_{t,n}(\mathcal{D}'_n)\|_1 \\ & = \sum_{k=1}^{23M} 2^{(k \bmod 23) - 23} |u_k - u'_k|. \end{aligned}$$

Due to inherent randomness, the bit-level distance between $\mathbf{u}_{t,n}$ and $\mathbf{u}'_{t,n}$ is non-deterministic, even with fixed \mathcal{D} , \mathcal{D}' , and $\omega_{t-1,n}$. It may occasionally reach the maximum value—an extreme and random case where all bits differ—yet the same configurations can still yield varying distances across repeated experiments.

Consider a single bit u_k , such as the k -th bit in the bitstream $\mathbf{u}_{t,n} \in \mathbb{B}^{23M \times 1}$, which is also the j -th fraction bit of a real number, where $j = (k \bmod 23)$. Due to inherent randomness, the bit-level difference between u_k and u'_k attains its maximum value (i.e., $2^{(k \bmod 23) - 23}$) with probability q_k , and equals zero with probability $1 - q_k$. The expectation of its bit-level distance between u_k and u'_k is $2^{(k \bmod 23) - 23} q_k$.

We now introduce a new metric, referred to as the sum of the expected bit-level distance of all bits between $\mathbf{u}_{t,n}$ and $\mathbf{u}'_{t,n}$ under a given classical sensitivity $\Delta\omega_{\max,n}$, denoted as

$$\bar{\kappa}_{\Delta\omega_{\max,n}} = \mathbb{E}(\kappa) = \sum_{k=1}^{23M} 2^{(k \bmod 23) - 23} q_k. \quad (15)$$

Remark 1. While the bit-level distances of these parameter pairs can vary significantly, $\bar{\kappa}_{\Delta\omega_{\max,n}}$ is introduced to characterize this variability. In the next section, we leverage Rényi divergence to quantify the privacy leakage risk, which has been proven to positively correlate with $\bar{\kappa}_{\Delta\omega_{\max,n}}$.

Note that directly using the maximum bit-level distance may overestimate the privacy risk, as it fails to capture the full distributional characteristics. This coarse approximation could lead to excessive differential privacy noise injection, thereby impairing the utility of the federated learning model.

Remark 2. For two bitstreams, the bit-level distance κ differs from the classical ℓ_1 -norm of the distance between the bitstreams. Consider two floating-point numbers \mathbf{a} and \mathbf{b} with the same sign and exponent parts, and different fraction parts, denoted by $(a_{22} \dots a_0)_2$ and $(b_{22} \dots b_0)_2$, respectively.

The ℓ_1 -norm is $|\sum_{j=0}^{22} 2^{j-23} (a_j - b_j)|$. By contrast, the bit-level distance is $\kappa = \sum_{j=0}^{22} 2^{j-23} |a_j - b_j|$, and is no smaller than the ℓ_1 -norm. As a consequence, given $\Delta\omega_{\max,n}$, $\bar{\kappa}_{\Delta\omega_{\max,n}}$ is no smaller than the expectation of the ℓ_1 -norm of the distance between any two bitstreams.

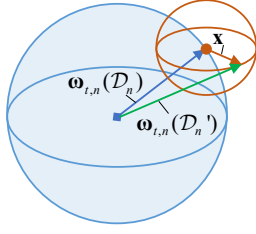


Fig. 2. An illustration of the model parameters $\omega_{t,n}(\mathcal{D}_n)$, $\omega_{t,n}(\mathcal{D}'_n)$, and \mathbf{x} . The blue sphere denotes the domain of the model parameters $\omega_{t,n}(\mathcal{D}_n)$. The red sphere denotes the domain of \mathbf{x} .

2) *Evaluation of $\bar{\kappa}_{\Delta\omega_{\max,n}}$* : To evaluate $\bar{\kappa}_{\Delta\omega_{\max,n}}$, we define $\mathbf{x} \in \mathbb{R}^{M \times 1}$ with $\mathbf{x} = \omega_{t,n}(\mathcal{D}_n) - \omega_{t,n}(\mathcal{D}'_n)$. Let x_m denote the m -th element of \mathbf{x} . Hence, $\|\mathbf{x}\|_2 = \sqrt{\sum_{m=1}^M |x_m|^2} = \Delta\omega_{\max,n}$. By definition, $\bar{\kappa}_{\Delta\omega_{\max,n}}$ can be written as

$$\bar{\kappa}_{\Delta\omega_{\max,n}} = \frac{\int \cdots \int_{\mathcal{R}} \bar{\kappa}(\omega + \mathbf{x}, \omega) d\omega_1 \cdots d\omega_M dx_1 \cdots dx_M}{\int \cdots \int_{\mathcal{R}} 1 d\omega_1 \cdots d\omega_M dx_1 \cdots dx_M}, \quad (16)$$

where $\mathcal{R} = \{(\omega_1, \cdots, \omega_M, x_1, \cdots, x_M)\}$ stands for the $2M$ -dimensional vector space satisfying

- The m -th element, ω_m , of the model parameter ω is in the range $\omega_m \in [-2^{(c_{30}c_{29} \cdots c_{23})_2 - 126}, 2^{(c_{30}c_{29} \cdots c_{23})_2 - 126}]$, $\forall m$;
- $\|\mathbf{x}\|_2 = \Delta\omega_{\max,n}$ achieves the classical sensitivity.

The nominator on the right-hand side (RHS) of (16) gives the volume of \mathcal{R} , and its reciprocal specifies the density, i.e., the probability distribution function (PDF), of \mathcal{R} .

Fig. 2 illustrates the defined vector space \mathcal{R} , using spheres to conceptualize regions defined by the ℓ_1 -norm for easier visualization. The volume of \mathcal{R} can be visualized as the total area of all the red spheres, each centered at every possible pair of vectors ω and \mathbf{x} . According to (13), $\sqrt{\sum_{m=1}^M |x_m|^2} = \frac{2\eta G}{|\mathcal{D}'_n|}$. $\bar{\kappa}_{\Delta\omega_{\max,n}}$ can be evaluated empirically at each device n based on its dataset \mathcal{D}_n ; see Section VII-A.

B. End-to-End (λ, ϵ) -Rényi DP

At the server, $\hat{\mathbf{u}}_{t,n}(\mathcal{D}_n)$ and $\hat{\mathbf{u}}_{t,n}(\mathcal{D}'_n)$ are the received bitstreams perturbed under the proposed bit-flipping DP mechanism with end-to-end BER $p_{t,n}$. The following theorem evaluates the end-to-end BER, denoted by $p_{t,n}$, ensuring that applying the bit-flipping DP mechanism to the binary model parameters of client n at the t -th round satisfies $(\lambda, \frac{\epsilon}{K})$ -Rényi DP. Furthermore, the proposed mechanism satisfies (λ, ϵ) -Rényi DP over K communication rounds.

Theorem 1. *With the expected bit-level distance $\bar{\kappa}_{\Delta\omega_{\max,n}}$ defined, applying the proposed bit-flipping mechanism $\mathcal{M}_{\text{BF}}(\mathbf{u}(\mathcal{D}_n), p_{t,n})$ defined in **Definition 2** for K communication rounds satisfies (λ, ϵ) -Rényi DP when the end-to-end BER is $p_{t,n} \geq \left(1 + \left(\frac{(\lambda-1)\epsilon}{K\bar{\kappa}_{\Delta\omega_{\max,n}}}\right)^{\frac{1}{\lambda-1}}\right)^{-1}$.*

Proof. The detailed proof can be found in **Appendix B**. \square

In Theorem 1, we analyze the privacy leakage risk using the Rényi divergence, based on the distributions of the received bitstreams corresponding to two adjacent datasets. To

quantify the influence of bit-level deviations, we introduce the expectation-based metric $\bar{\kappa}_{\Delta\omega_{\max,n}}$, which captures the joint impact of the maximum bit-level distance and its probability on privacy leakage. We further demonstrate that the Rényi divergence is positively correlated to $\bar{\kappa}_{\Delta\omega_{\max,n}}$, by establishing an upper bound involving the one-round privacy budget $\frac{\epsilon}{K}$. This facilitates analyzing the end-to-end BER $p_{t,n}$.

Remark 3. *The above analysis does not consider encryption. Nevertheless, it can be extended to systems where devices encrypt their local models before bit-flipping and transmissions.*

In the case of non-diffusion encryption methods, e.g., certain stream ciphers and the one-time pad, each bit or byte of the plaintext is directly transformed through linear operations, e.g., XOR. Bit errors in the ciphertext mirror those in the corresponding positions of the decrypted plaintext. The BER of the ciphertext is consistent with the BER of the decrypted plaintext, i.e., $p_{t,n} \triangleq p_{t,n}^{\text{PT}} = p_{t,n}^{\text{CT}}$ with $p_{t,n}^{\text{PT}}$ and $p_{t,n}^{\text{CT}}$ being the BERs of the plaintext and ciphertext, respectively.

In the case of diffusion encryption methods, e.g., AES and DES, a fixed block size of 128 or 64 bits is typically used. The methods are engineered to propagate the impact of bit errors across entire blocks. Even a single bit error can corrupt an entire block, leading to widespread bit errors. The BER of the plaintext within the block is expected to be 0.5 to make the original plaintext irrecoverable. Taking AES with a block size of 128 bits as an example. When the BER of the ciphertext is $p_{t,n}^{\text{CT}}$, the block error rate of a received block is $1 - (1 - p_{t,n}^{\text{CT}})^{128}$. Then, the BER of the decrypted plaintext is 0.5 when one or more bit errors are in the received block of the ciphertext. When there is no error in the ciphertext block, the BER of the decrypted plaintext is 0. Based on the Law of Total Probability, the BER of the decrypted plaintext $p_{t,n}$ is

$$p_{t,n} \triangleq p_{t,n}^{\text{PT}} = (1 - (1 - p_{t,n}^{\text{CT}})^{128}) \times 0.5 + (1 - p_{t,n}^{\text{CT}})^{128} \times 0. \quad (17)$$

According to (38), we have $p_{t,n}^{\text{CT}} = 1 - (1 - 2p_{t,n})^{\frac{1}{128}}$.

In both cases, the BERs of the decrypted plaintext, $p_{t,n}^{\text{PT}}$, can be evaluated and substituted into (38) to help specify the end-to-end BER of the proposed bit-flipping DP mechanism.

VI. CONVERGENCE ANALYSIS

In this section, we analyze the convergence of WFL under the proposed bit-flipping mechanism. Due to the artificial bit-flipping noise and communication noise, $\tilde{\omega}_{t,n}$, $\forall n$ is likely to be imprecise. We define $\mathbf{z}_{t,n}$ as the local bias between the locally updated model of device n and the corresponding model recovered at the server, i.e., $\omega_{t,n}$ and $\tilde{\omega}_{t,n}$:

$$\mathbf{z}_{t,n} = \tilde{\omega}_{t,n} - \omega_{t,n}. \quad (18)$$

The global bias between the ideal global model, i.e., $\sum_{n \in \mathcal{N}} q_n \omega_{t,n}$, and the corresponding imperfect global model, i.e., $\omega_{t,G} = \sum_{n \in \mathcal{N}} q_n \tilde{\omega}_{t,n}$, can be defined as

$$\mathbf{z}_{t,G} = \sum_{n \in \mathcal{N}} q_n (\tilde{\omega}_{t,n} - \omega_{t,n}) = \sum_{n \in \mathcal{N}} q_n \mathbf{z}_{t,n}. \quad (19)$$

Lemma 2. *With the mean and variance of a bitstream with randomly flipped bits given in **Lemma 1**, the local and global biases, $\mathbf{z}_{t,n}$, $\forall n$ and $\mathbf{z}_{t,G}$, have the following properties:*

1) The expectation and variance of $\mathbf{z}_{t,n}$ are given by

$$\mathbb{E}(\mathbf{z}_{t,n}) \approx 2p_{t,n}\boldsymbol{\omega}_{t,n}; \quad (20)$$

$$\mathbb{E}(\|\mathbf{z}_{t,n} - \mathbb{E}(\mathbf{z}_{t,n})\|_2^2) = \frac{(1-4^{-23})}{3} M p_{t,n} (1-p_{t,n}) \times 2^{2(c_{30}c_{29}\dots c_{23})_2 - 250}. \quad (21)$$

2) The ℓ_2 -norm of the global bias $\mathbf{z}_{t,G}$, i.e., $\|\mathbf{z}_{t,G}\|_2^2$, is upper bounded by

$$\mathbb{E}(\|\mathbf{z}_{t,G}\|_2^2) \leq \frac{(1-4^{-23})M}{3} \sum_{n \in \mathcal{N}} q_n^2 p_{t,n} (1-p_{t,n}) \times 2^{2(c_{30}c_{29}\dots c_{23})_2 - 250} + \sum_{n \in \mathcal{N}} q_n p_{t,n} \nu_2^2 \triangleq X_t^{\text{BF}}(G, \nu_2, \nu_\infty). \quad (22)$$

where $X_t^{\text{BF}}(G, \nu_2, \nu_\infty)$ depends on $\nu_\infty = (c_{31}c_{30}\dots c_0)_2$ since $c_{30}c_{29}\dots c_{23}$ are the exponent bits of ν_∞ . $X_t^{\text{BF}}(G, \nu_2, \nu_\infty)$ is positively related to G , ν_2 and ν_∞ .

Proof. See **Appendix C**. \square

Remark 4 (Comparison with the Gaussian Mechanism). When utilizing the Gaussian Mechanism to achieve the (ϵ, δ) -DP, the expectation and variance of $\mathbf{z}_{t,n}$ are

$$\mathbb{E}(\mathbf{z}_{t,n}) = 0 \quad \text{and} \quad \mathbb{E}(\|\mathbf{z}_{t,n} - \mathbb{E}(\mathbf{z}_{t,n})\|_2^2) = M\sigma_n^2, \quad (23)$$

where $\sigma_n = \frac{\Delta\omega_n K \sqrt{2 \ln(1.25/\delta)}}{\epsilon}$ is the Gaussian variance [36].

The ℓ_2 -norm of the global bias is upper bounded by

$$\mathbb{E}(\|\mathbf{z}_{t,G}\|_2^2) \leq \sum_{n \in \mathcal{N}} q_n^2 M \frac{(\Delta\omega_{\max,n} K)^2 2 \ln(\frac{1.25}{\delta})}{\epsilon^2} = \sum_{n \in \mathcal{N}} q_n^2 M \frac{(2\eta GK)^2 \times 2 \ln(1.25/\delta)}{|\mathcal{D}_n|^2 \epsilon^2} \triangleq X_t^{\text{Gauss}}(G). \quad (24)$$

When the privacy budget, i.e., ϵ , and the FL hyperparameters, e.g., $\bar{\kappa}_{\Delta\omega_{\max}}$, $\Delta\omega$, and K , are given, one can choose the suitable mechanism, e.g., the proposed bit-flipping mechanism or the Gaussian mechanism, by numerically comparing the ℓ_2 -norm of the global bias under the two mechanisms, i.e., (22) and (24). The bit-flipping mechanism may enjoy a relatively larger privacy budget since it can leverage the communication noise to spare some privacy budget for bit-flipping.

Next, we proceed to analyze the convergence of WFL under the proposed bit-flipping DP mechanism. Recall a total of $T < \infty$ training iterations, with E local iterations per communication round. For illustration convenience, we consider full-batch gradient descent in this paper⁵.

Assumption 1. Some widely used assumptions for analyzing convergence bounds for FL are considered:

- 1) There exist such two constants $\mu > 0$ and $\alpha > 0$ that per any device n , the local loss function $F_n(\mathbf{w})$, $\forall n$ is μ -strongly convex and α -smooth, i.e., $\alpha \|\mathbf{w}_1 - \mathbf{w}_2\|_2 \geq \|\nabla F_n(\mathbf{w}_1) - \nabla F_n(\mathbf{w}_2)\|_2 \geq \mu \|\mathbf{w}_1 - \mathbf{w}_2\|_2$, $\forall \mathbf{w}_1, \mathbf{w}_2 \in \mathbb{R}^{M \times 1}$. Subsequently, the global loss function $F(\mathbf{w})$ is μ -strongly convex and α -smooth.
- 2) As assumed in [41], the variances of stochastic gradients are bounded by $\mathbb{E}_{\xi_{t,n}}(\|\nabla F_n(\mathbf{w}_{t,n}, \xi_{t,n}) -$

$\nabla F_n(\mathbf{w}_{t,n})\|_2^2) \leq \sigma_n^2$, $\forall n, t$, where $\xi_{t,n}$ is the mini-batch of device n in the i -th iteration of round t . Considering full-batch gradient, in this paper, $\sigma_n^2 = 0$.

Definition 3. For convergence analysis,

- 1) Define two virtually aggregated models at the t -th iteration as $\bar{\boldsymbol{\omega}}_t = \sum_{n \in \mathcal{N}} q_n \boldsymbol{\omega}_{t,n}$ and $\bar{\mathbf{w}}_t = \sum_{n \in \mathcal{N}} q_n \mathbf{w}_{t,n}$; see (3) and (4), respectively. $\bar{\boldsymbol{\omega}}_t = \bar{\mathbf{w}}_t$, if $t \notin \mathcal{I}_E$; $\bar{\mathbf{w}}_t = \bar{\boldsymbol{\omega}}_t + \mathbf{z}_{t,G}$, if $t \in \mathcal{I}_E$.
- 2) Let $\Gamma = F^* - \sum_{n \in \mathcal{N}} q_n F_n^*$ be the global heterogeneity degree to capture the heterogeneity of the local datasets.

Under **Assumption 1**, the convergence upper bound of WFL under the proposed bit-flipping mechanism is established by analyzing $\|\bar{\mathbf{w}}_t - \mathbf{w}^*\|_2^2$, which is the distance between $\bar{\mathbf{w}}_t$, i.e., the virtually aggregated model at the t -th training iteration, and \mathbf{w}^* , i.e., the optimal global model, as stated in the following.

Theorem 2. Given T and E , the convergence upper bound of WFL under the bit-flipping mechanism is given by

$$\mathbb{E}(\|\bar{\mathbf{w}}_T - \mathbf{w}^*\|_2^2) \leq \zeta_1 \|\bar{\mathbf{w}}_0 - \mathbf{w}^*\|_2^2 + \zeta_2 \eta^2 B + \zeta_3 \frac{X^{\text{BF}}(G, \nu_2, \nu_\infty)}{\sqrt{p_{\max}}}, \quad (25)$$

where the expectation \mathbb{E} is taken over the random bit-flipping noise across all communication rounds;

$$\zeta_1 = (1 + \sqrt{p_{\max}})^K (1 - \eta\mu)^T;$$

$$\zeta_2 = \frac{1 - (1 - \eta\mu)^T (1 + \sqrt{p_{\max}})^K}{1 - (1 - \eta\mu)^E (1 + \sqrt{p_{\max}})} (1 + \sqrt{p_{\max}}) \frac{1 - (1 - \eta\mu)^E}{\eta\mu};$$

$$\zeta_3 = \frac{1 - (1 - \eta\mu)^T (1 + \sqrt{p_{\max}})^K}{1 - (1 - \eta\mu)^E (1 + \sqrt{p_{\max}})} (1 + \sqrt{p_{\max}});$$

$$p_{\max} = \max_{\forall t, n \in \mathcal{N}} p_{t,n}; \quad B = 6\alpha\Gamma + 8(E-1)^2 G^2;$$

$$X^{\text{BF}}(G, \nu_2, \nu_\infty) = \max_{\forall t} X_t^{\text{BF}}(G, \nu_2, \nu_\infty).$$

Proof. See **Appendix D**. \square

When the bit-flipping noise (resulting from both the artificial noise and noisy wireless channels) is small enough, i.e., $p_{\max} \rightarrow 0$ and $X^{\text{BF}} \rightarrow 0$, the convergence upper bound in (25) tends to $\mathbb{E}(\|\bar{\mathbf{w}}_T - \mathbf{w}^*\|_2^2) \leq (1 - \eta\mu)^T \|\bar{\mathbf{w}}_0 - \mathbf{w}^*\|_2^2 + \eta^2 B \frac{1 - (1 - \eta\mu)^T}{\eta\mu}$, which is consistent with the upper bound of the existing baseline developed with no privacy consideration in [41]. The validity of (25) is cross-verified. In addition, $X^{\text{BF}}(G, \nu_2, \nu_\infty)$ can be replaced by $X^{\text{Gauss}}(G) = \max_{\forall t} X_t^{\text{Gauss}}(G)$ in (25) under the Gaussian mechanism.

Moreover, the first term on the RHS of (25) shows the dominant impact of the increasing number of training iterations, which decreases and converges to zero with the increase of T . The second term accounts for the data heterogeneity of the participating devices. The third term of (25) captures the impact of the bit-flipping noise on the convergence and tends to zero when no DP noise is considered. All terms on the RHS of (25) consist of the maximum noise level p_{\max} , which penalizes the utility of WFL. Particularly, the first term may fail to converge when $(1 + \sqrt{p_{\max}})(1 - \eta\mu)^E > 1$, resulting from a reduction of the privacy budget and further enlarging the end-to-end BER. The other terms on the RHS of (25)

⁵The convergence and privacy analysis under full-batch gradient descent can be extended to the mini-batch setting by accounting for the reduced exposure of individual samples and the stochastic nature of sampling [4], [37]–[40].

increase with p_{\max} . To this end, it is imperative to control the increase of p_{\max} to balance the privacy and utility of FL.

Remark 5 (Impact of clipping threshold). *Selecting an appropriate gradient clipping threshold G is crucial. If G is too small, the WFL convergence can significantly slow down [13], [29]. If G is too large, the ℓ_∞ -norm of the clipped gradient vector ν_∞ would increase the convergence upper bound and penalize the accuracy of WFL. This is due to the fact that $X^{\text{BF}}(G, \nu_2, \nu_\infty)$ in (25) is positively related to both ν_2 and ν_∞ . Typically, G is specified empirically. With reference to [4], [14], in this paper, we set G as the median of the ℓ_2 -norms of the unclipped gradient obtained during training.*

VII. EXPERIMENTS AND EVALUATIONS

In this section, we conduct extensive experiments to validate the convergence analysis of the proposed channel-native bit-flipping mechanism for privacy-preserving WFL.

A. Estimation of Bit-Level Distance

It is non-straightforward to analytically derive the proposed expected bit-level distance $\bar{\kappa}_{\Delta\omega_{\max}}$ in (16), due to the lack of the *a-priori* knowledge about the continuous domain \mathcal{R} . Nevertheless, each device can readily estimate its expected bit-level distance $\bar{\kappa}_{\Delta\omega_{\max}}$ within a practical discrete domain sampled from the continuous domain \mathcal{R} . Specifically, each device can pre-train its local model parameters and collect a set of model parameters, denoted as \mathcal{W} . It can also create a set of $\mathcal{X} = \{\mathbf{x} \mid \|\mathbf{x}\|_2 = \Delta\omega_{\max}\}$ comprising a large number of samples (*e.g.*, 10,000 samples in our experiments) randomly selected from the M -dimensional vector space satisfying $\|\mathbf{x}\|_2 = \Delta\omega_{\max}$. Then, the device can estimate the expected bit-level distance $\bar{\kappa}_{\Delta\omega_{\max}}$, as given by

$$\bar{\kappa}_{\Delta\omega_{\max}} = \frac{\sum_{\mathbf{x} \in \mathcal{X}, \omega \in \mathcal{W}} \kappa(\omega_1, \dots, \omega_M, x_1, \dots, x_M)}{\sum_{\mathbf{x} \in \mathcal{X}, \omega \in \mathcal{W}} 1}, \quad (26)$$

which is a discrete approximation of (16).

Fig. 3 evaluates the impacts of the model size M and the classical sensitivity $\Delta\omega_{\max}$ on the estimated expected bit-level distance $\bar{\kappa}_{\Delta\omega_{\max}}$. In general, $\bar{\kappa}_{\Delta\omega_{\max}}$ grows with M and $\Delta\omega_{\max}$, while exhibiting some fluctuations. This is because, given $\Delta\omega_{\max}$, enlarging M increases the ℓ_1 -norms of the distances between bitstreams. Then, $\bar{\kappa}_{\Delta\omega_{\max}}$ also increases, since $\bar{\kappa}_{\Delta\omega_{\max}}$ is no smaller than the expectation of the ℓ_1 -norms; see **Remark 2**.

B. Evaluation of Bit-Flipping DP for WFL

By default, we set the communication BER, $p_{t,n,C}$, to be randomly and uniformly distributed within $[0, 0.02]$. When the bit-flipping DP mechanism is in use, the end-to-end and the artificial BERs are generated using **Algorithm 1**.

1) *ML Model and Dataset*: We consider the following two ML models and two widely used public datasets.

- **CNN & F-MNIST**: We consider an image classification task to classify a non-identical and independently distributed (non-i.i.d.) F-MNIST dataset based on a CNN model. The CNN model has two convolutional layers with 32 or 64

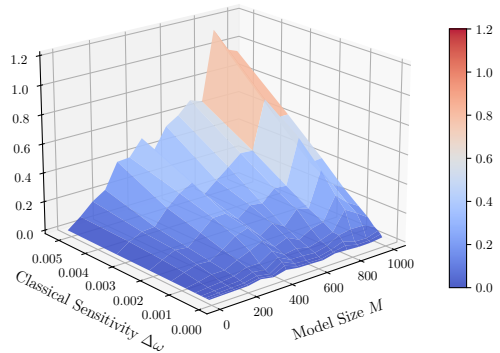


Fig. 3. Estimated expected bit-level distance $\bar{\kappa}_{\Delta\omega_{\max}}$ versus model parameter size M and classical sensitivity $\Delta\omega_{\max}$.

convolutional filters per layer. The size of the CNN model is $M = 1.21 \times 10^6$. The F-MNIST dataset has 671,585 training examples, 77,483 testing examples and 62 labels. There are 20 devices, each randomly selecting $|\mathcal{D}_n| = 2,000$ training examples with 10 labels. The local learning rate is $\eta = 0.1$. By default, the gradient clipping threshold is $G = 1$. We can empirically obtain $\nu_2 = 16$ and $\nu_\infty = 0.5$ by evaluating the ℓ_2 - and ℓ_∞ -norms of the updated model parameters. With reference to [4], [14], we set G as the median of the norms of the unclipped gradient throughout training. The classical sensitivity is $\Delta\omega_{\max} = 10^{-4}$. The expected bit-level distance is estimated to be $\bar{\kappa}_{\Delta\omega_{\max}} = 0.02$, as described in Section VII-A.

- **ResNet18 & Fed-CIFAR100**: Another image classification task is to train the ResNet18 model on the Fed-CIFAR100 dataset. The ResNet18 model has 18 layers, including 17 convolutional layers and a fully connected layer. Compared to a plain CNN model, the ResNet model inserts shortcut connections to prevent vanishing gradients [42]. The size of the ResNet18 model is $M = 11.69 \times 10^6$. Fed-CIFAR100 divides the standard CIFAR100 into 10 training subsets with 10 image classes per subset. Each image has 32×32 pixels. There are 10 devices, each training the image samples of all 10 classes, a total of $|\mathcal{D}_n| = 2,000$ images. The learning rate is $\eta = 1$. The default clipping threshold is $G = 1$, and correspondingly, $\nu_2 = 128$ and $\nu_\infty = 1$. The classical sensitivity is $\Delta\omega_{\max} = 10^{-3}$. Then, the expected bit-level distance is estimated to be $\bar{\kappa}_{\Delta\omega_{\max}} = 0.025$.

2) *Benchmarks*: We also implement the following channel-agnostic baselines to serve as the benchmarks.

- **Channel-agnostic bit-flipping mechanism**: The artificial bit-flipping noise generated by (λ, ϵ) -Rényi DP (see Sections IV-A and IV-B1) is employed solely for privacy protection, *i.e.*, $p_{t,n,A} = p_{t,n}$. It does not exploit the communication noise for privacy protection.

- **Channel-agnostic Gaussian mechanism (with erroneous packets accepted)**: The local models are solely protected by artificial Gaussian noise satisfying (ϵ, δ) -DP [14]. The communication noise may flip the sign and exponent bits of **binary32** numbers, compromising the convergence of WFL.

- **Channel-agnostic Gaussian mechanism with erroneous**

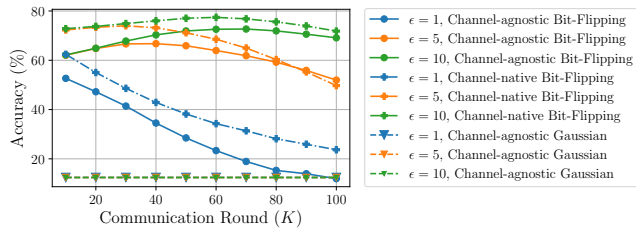


Fig. 4. Comparison of the proposed channel-native mechanism with channel-agnostic mechanisms suffering from bit-flipping communication noises. $\bar{\kappa}\Delta\omega_{\max} = 0.02$; $\Delta\omega_{\max} = 10^{-4}$; $E = 50$; and $\lambda = 2$.

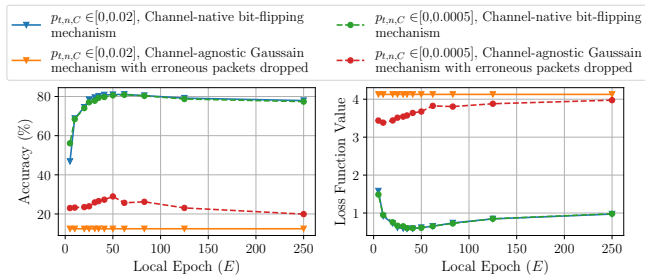


Fig. 5. Comparison of the proposed bit-flipping mechanism with channel-agnostic Gaussian mechanism suffering from erroneous packets dropped. $\epsilon = 10$; $T = 2,500$; and $\lambda = 2$.

packets dropped: Different from the channel-agnostic Gaussian mechanism, the local models of a device are segmented and packetized. The standard WiFi packet of 2,312 bytes is considered. Each packet is encoded with a circular redundancy check, and discarded at the server if it fails to pass the check. This mechanism represents the state of the art.

In the baselines using the Gaussian mechanism, the DP noise scale is $\sigma = \frac{\Delta\omega_{\max}K\sqrt{2\ln(1.25/\delta)}}{\epsilon'}$ satisfying (ϵ', δ) -DP [36]. For a fair comparison, (λ, ϵ) -Rényi DP can be equivalently converted into (ϵ', δ) -DP, with $\delta = \frac{e^{(\lambda-1)(\epsilon-\epsilon')}}{\lambda-1} (1 - \frac{1}{\lambda})^\lambda$ [43]. In this paper, we set $\epsilon = \epsilon'$ by default.

3) Comparison with Channel-Agnostic DP Mechanisms:

Fig. 4 evaluates the impact of different DP mechanisms on the accuracy of WFL in a noisy wireless environment. The proposed channel-native bit-flipping mechanism outperforms all channel-agnostic mechanisms, since it takes advantage of the noisy nature of wireless channels for privacy protection. By contrast, the channel-agnostic schemes overlook the privacy-preserving capability offered by wireless channels, and hence, suffer from excessive privacy protection at the cost of accuracy.

The proposed bit-flipping mechanism outperforms the Gaussian mechanisms, even when it overlooks the privacy-preserving capability of noisy wireless channels, thanks to the new floating-point-to-fixed-point conversion method. This is because all bits in **binary32** are transmitted in the channel-agnostic Gaussian mechanism, and their sign and exponent bits can have errors and dramatically distort the local models. By contrast, only the fraction bits are transmitted under the proposed approach, with 28% lower traffic than the channel-agnostic Gaussian mechanism, benefiting from the floating-point-to-fixed-point conversion; see Section IV-A.

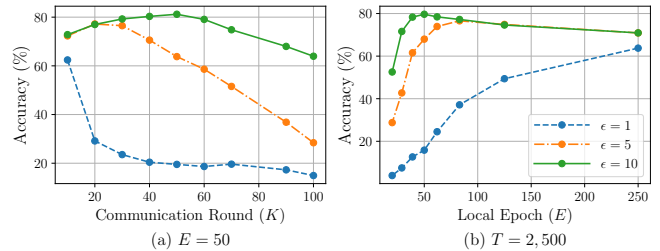


Fig. 6. Accuracy of CNN on F-MNIST versus K and E . $\lambda = 2$.

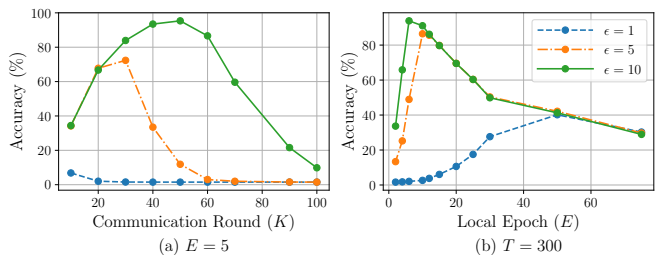


Fig. 7. Accuracy of ResNet18 model on Fed-CIFAR100 dataset versus K , E and ϵ , where $\lambda = 2$.

Fig. 5 compares the proposed channel-native bit-flipping mechanism with the channel-agnostic Gaussian mechanism under a more classical setting with any erroneous packets dropped at the server. The standard WiFi packet length of 2,312 bytes is considered. Both mechanisms experience the same channel conditions with the same communication BER, $p_{t,n,C}$, distributed uniformly randomly within the default range $[0, 0.02]$ and within the range $[0, 0.0005]$. The proposed mechanism is significantly better, indicating that even erroneous local models corrupted by channel fading and noise can still contain useful model information and can be aggregated to improve the convergence and accuracy of WFL.

4) *Impact of Parameters:* Fig. 6 plots the accuracy of the CNN model on the F-MNIST dataset. Fig. 7 plots the accuracy of ResNet18 on the Fed-CIFAR100 dataset. It is demonstrated in both figures that increasing the privacy budget ϵ leads to a decrease in the end-to-end BER, thereby improving the accuracy of WFL under the mechanism.

Figs. 6(a) and 7(a) examine the impact of the number of local epochs E on the utility of two image classification tasks, respectively. It is observed that the optimal value of E exists within the given range. This is because a larger E reduces the number of communication rounds, *i.e.*, K , when the total number of iterations, T , is given, thereby alleviating the impact of the bit-flipping noise on the training accuracy of WFL under the proposed bit-flipping DP mechanism. On the other hand, in the face of the heterogeneity of the local datasets, a larger E can cause the local models to be biased towards the local data of the clients, resulting in poor global training performance.

Figs. 6(b) and 7(b) evaluate the proposed DP mechanism, where T varies while E remains unchanged. The efficiency of the image classification tasks initially increases and then decreases, as T increases. The underlying reason is two-fold. On the one hand, a decrease in T leads to a decrease in the end-to-end BER, $p_{t,n}$, benefiting the convergence of WFL. On the

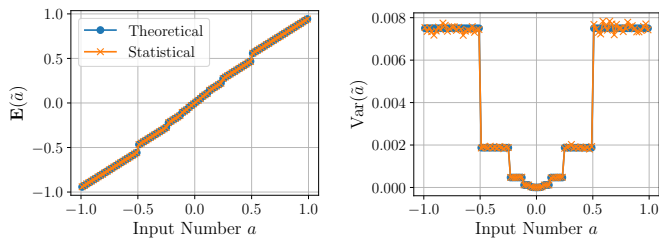


Fig. 8. The statistical properties of perturbed values \tilde{a} vs. original numbers a , where the bit-flipping probability is $p = 0.1$ and we show $a \in [-1, +1]$ for the clarity of the figure.

other hand, an increase of T allows for more local iterations and global aggregations, improving the accuracy of WFL. In this sense, the optimal T exists in the proposed mechanism.

As T keeps increasing, the end-to-end BER, $p_{t,n}$, increases and converges to 0.5. In this case, the local models are severely corrupted by the artificial and communication noises and become nearly completely random. As a consequence, WFL training cannot even start properly.

C. Statistical Properties of Bit-Flipping

Fig. 8 shows the consistency between the analytical and empirical results of the mean and variance of \tilde{a} . The validity of **Lemma 1** is confirmed. As shown in Fig. 8(a), the mean of \tilde{a} is linear in the range of the original floating-point numbers with the same sign and exponent parts, which is consistent with (5). As shown in Fig. 8(b), the variance of \tilde{a} does not change with a in the range with the same sign and exponent parts, which is consistent with (6). These phenomena can be observed across $a \in [-\infty, \infty]$.

VIII. CONCLUSION

This paper proposed a novel channel-native bit-flipping DP mechanism that exploits inherent noise in wireless channels to preserve the privacy of WFL. Specifically, we proposed a new floating-point-to-fixed-point conversion method, which only requires the bits in the fraction part of model parameters to be transmitted and hence prevents dramatic model distortions that would otherwise occur when transmitting floating-point numbers, *e.g.*, IEEE 754 **binary32**. We also analyzed the expected bit-level distance of the model parameters, and proved rigorously that the proposed mechanism satisfies (λ, ϵ) -Rényi DP and facilitates WFL convergence. Extensive experimental evaluations of two image classification tasks demonstrated the superiority of the proposed mechanism compared to the state-of-the-art channel-agnostic Gaussian mechanisms.

APPENDIX

A. Proof of Lemma 1

We start by proving (5). After flipping the bits in the fraction part of a with probability p (resulting from the bit-flipping perturbation and receiver noise), the probability of each received bit, $\tilde{a}_i, i = 0, 1, \dots, 22$, is given by

$$\Pr(\tilde{a}_i|a_i) = \begin{cases} 1-p, & \text{if } a_i \text{ is received correctly;} \\ p, & \text{otherwise,} \end{cases}$$

Then, the expectation of each received bit is given by

$$\mathbb{E}(\tilde{a}_i) = (1-p)a_i + p(1-a_i) = a_i(1-2p) + p.$$

The (decimal) mean of $\tilde{a} = (\tilde{a}_{22}\tilde{a}_{21}\dots\tilde{a}_0)_2$ is given by

$$\mathbb{E}(\tilde{a}) = (-1)^{a_{31}} 2^{(a_{30}a_{29}\dots a_{23})_2 - 127} \left(1 + \sum_{i=1}^{23} \mathbb{E}(\tilde{a}_{23-i}) 2^{-i} \right). \quad (27)$$

By plugging $\mathbb{E}(\tilde{a}_i) = a_i(1-2p) + p$ into (27), $\mathbb{E}(\tilde{a})$ becomes

$$\mathbb{E}(\tilde{a}) = (1-2p)a + (-1)^{a_{31}} 2^{(a_{30}a_{29}\dots a_{23})_2 - 127} \left(2p + \sum_{i=1}^{23} 2^{-i} p \right),$$

which leads to (5). Next, we prove (6). After flipping the fraction part of a with probability p , the variance of each bit is $\text{Var}(\tilde{a}_i) = p(1-p), i = 0, \dots, 22$. Then, the (decimal) variance of the bit-flipping value is given by

$$\begin{aligned} \text{Var}(\tilde{a}) &= \left((-1)^{a_{31}} 2^{(a_{30}a_{29}\dots a_{23})_2 - 127} \right)^2 \sum_{i=1}^{23} p(1-p) 2^{-2i} \\ &= \frac{(1-4^{-23})}{3} p(1-p) \left(2^{(a_{30}a_{29}\dots a_{23})_2 - 127} \right)^2, \end{aligned} \quad (28)$$

which leads to (6).

B. Proof of Theorem 1

For conciseness, we suppress the subscripts “ t ” and “ n ” from $p_{t,n}$, $\mathbf{u}_{t,n}$, \mathcal{D}_n , $\Delta\omega_{\max,n}$, and $\bar{\kappa}_{\Delta\omega_{\max,n}}$ in the rest of this section. The bit-flipping DP mechanism applied to the local model parameters $\mathbf{u} \in \mathbb{B}^{23M \times 1}$ adheres to $(\lambda, \frac{\epsilon}{K})$ -Rényi DP, and satisfies

$$D_\lambda(Q_{\mathbf{u}} \| Q_{\mathbf{u}'}) = \sum_{k=1}^{23M} D_\lambda(Q_{k,u_k}[\rho_k] \| Q_{k,u'_k}[\rho_k]) \leq \frac{\epsilon}{K}, \quad (29)$$

where the Rényi divergence $D_\lambda(Q_{\mathbf{u}} \| Q_{\mathbf{u}'})$ is based on the composition of independently applying the bit-flipping mechanism to each bit of the bitstream, incorporating the corresponding significance (binary weight) $2^{(k \bmod 23) - 23}$ of the k -th bit; $Q_{\mathbf{u}}$ and $Q_{\mathbf{u}'}$ denote the output distribution after applying bit-flipping mechanism to \mathbf{u} and \mathbf{u}' , respectively; $D_\lambda(Q_{k,u_k}[\rho_k] \| Q_{k,u'_k}[\rho_k])$ is the Rényi divergence of k -th bit:

$$D_\lambda(Q_{k,u_k}[\rho_k] \| Q_{k,u'_k}[\rho_k]) \triangleq \frac{1}{\lambda-1} \ln \left[\mathbb{E}_{\rho_k \sim Q_{k,u_k}[\rho_k]} \left(\frac{Q_{k,u_k}[\rho_k]}{Q_{k,u'_k}[\rho_k]} \right)^\lambda \right], \quad (30)$$

where ρ_k denotes the resultant decimal representation after flipping the k -th bit u_k (or u'_k) in the received bitstream, *i.e.*, $\rho_k = \sum_{i=0}^{22} 2^{i-23} \rho_i$, and $\rho_{(k \bmod 23)} \triangleq \hat{u}_k$ (or \hat{u}'_k) denotes the received version of u_k (or u'_k), which may have been flipped. The remaining bits $\rho_i, \forall i \neq (k \bmod 23)$, are assumed to be independently perturbed with unknown distributions. $Q_{k,u_k}[\rho_k]$ and $Q_{k,u'_k}[\rho_k]$ are the probability mass functions (PMFs) of the decimal representation ρ_k after randomly flipping \hat{u}_k and \hat{u}'_k , respectively, each weighted by $2^{(k \bmod 23) - 23}$, assuming all other bits are varied independently and treated as unknown. $D_\lambda(\cdot \| \cdot)$ denote Rényi divergence of order λ . $\mathbb{E}_{\rho_k \sim Q_{k,u_k}[\rho_k]} \left(\frac{Q_{k,u_k}[\rho_k]}{Q_{k,u'_k}[\rho_k]} \right)^\lambda$ is the key term of Rényi divergence.

Suppose that the bit-level difference between u_k and u'_k attains its maximum value (*i.e.*, $2^{(k \bmod 23) - 23}$) with probability q_k , or zero with probability $1 - q_k$. Then, the expectation of its bit-level distance between u_k and u'_k is $2^{(k \bmod 23) - 23} q_k$.

Now, we can introduce an auxiliary bitstream $\mathbf{b} \in \mathbb{B}^{23M \times 1}$. The k -th bit of its fraction part, b_k , differs from u'_k with the maximum bit-level distance, with probability 1. Let $Q_{k,b_k}[\rho_k]$ denote the PMFs of the decimal representations ρ_k after

undergoing the bit-flipping operation on b_k . Based on the auxiliary distribution $Q_{k,b_k}[\rho_k]$ and $Q_{k,u'_k}[\rho_k]$, the output of $Q_{k,u_k}[\rho_k]$ is a mixed distribution:

$$Q_{k,u_k}[\rho_k] = q_k Q_{k,b_k}[\rho_k] + (1 - q_k) Q_{k,u'_k}[\rho_k]. \quad (31)$$

Next, we factor in the weight $2^{(k \bmod 23) - 23}$ corresponding to the k -th fraction bit. Since only the fraction parts are encoded into the bitstream, u'_k and b_k correspond to the m -th decimal number ($m = \lfloor \frac{k}{23} \rfloor$) of the model parameter vector, i.e., $\mathbf{u}'_m = \sum_{i=0}^{22} u'_{i+23m} 2^{i-23}$ and $\mathbf{b}_m = \sum_{i=0}^{22} b_{i+23m} 2^{i-23}$. Clearly, both \mathbf{u}'_m and \mathbf{b}_m lie within the range $[0, 1)$.

Then, we evaluate the probability of distinguishing between the pair $(\mathbf{u}'_m, \mathbf{b}_m)$ when only u'_k and b_k are independently considered. Since the other bits of \mathbf{u}'_m and \mathbf{b}_m are independent and unknown, the resolution with which the real number can be identified is $2^{(k \bmod 23) - 23}$. We divide the range $[0, 1)$ into $2^{23 - (k \bmod 23)}$ intervals. Each interval collects the numbers whose fraction parts share identical bits from the 22nd bit down to the $(k \bmod 23)$ -th bit, while the bits from position $(k \bmod 23) - 1$ down to 0 may vary and its distribution are unknown. In particular, \mathbf{u}'_m and \mathbf{b}_m correspond to two distinct intervals, $\mathbf{X}_{\mathbf{u}'_m}$ and $\mathbf{X}_{\mathbf{b}_m}$, respectively. The other intervals indicate the distribution of the other bits ($i \neq k \bmod 23$) being flipped or not, which does not contribute to distinguishing between the pair $(\mathbf{u}'_m, \mathbf{b}_m)$.

Without loss of generality, we analyze the output distribution of the decimal representation of \hat{u}'_k after applying the bit-flipping operation to u'_k with probability p .

- The probability that the received value \hat{u}'_k equals b_k is p . Since the other bits are governed by independent mechanisms and treated as unknown, the distribution of the decimal representation of \hat{u}'_k must rely on random guessing for the remaining bits. Consequently, the probability that the interval $\mathbf{X}_{\mathbf{b}_m}$, corresponding to the decimal representation ρ_k , aligns with that of \mathbf{b}_m is $2^{(k \bmod 23) - 23} \cdot p$.
- The received value \hat{u}'_k remains u'_k with probability $1 - p$. Consequently, the probability that the interval $\mathbf{X}_{\mathbf{u}'_m}$, corresponding to the decimal representation ρ_k of \hat{u}'_k , aligns with that of \mathbf{u}'_m is $2^{(k \bmod 23) - 23} \cdot (1 - p)$.
- When the decimal representation of \hat{u}'_k falls into intervals other than $\mathbf{X}_{\mathbf{b}_m}$ and $\mathbf{X}_{\mathbf{u}'_m}$, it does not help distinguish between the pair $(\mathbf{u}'_m, \mathbf{b}_m)$. The probability of any of these intervals is $2^{(k \bmod 23) - 23}$, and the total probability of falling into these indistinguishable intervals is $1 - 2^{(k \bmod 23) - 23}$.

By summarizing the above three cases, the overall distribution of $\rho_k \sim Q_{k,u'_k}[\rho_k]$ is given by

$$Q_{k,u'_k}[\rho_k] = \begin{cases} \Pr(\rho_k \in \mathbf{X}_{\mathbf{b}_m}) = 2^{(k \bmod 23) - 23} \cdot p; \\ \Pr(\rho_k \in \mathbf{X}_{\mathbf{u}'_m}) = 2^{(k \bmod 23) - 23} \cdot (1 - p); \\ \Pr(\rho_k \in [0, 1) \setminus \mathbf{X}_{\mathbf{b}_m} \setminus \mathbf{X}_{\mathbf{u}'_m}) = 1 - 2^{(k \bmod 23) - 23}. \end{cases} \quad (32)$$

By following the same analysis steps, the distribution of $Q_{k,b_k}[\rho_k]$ is given by

$$Q_{k,b_k}[\rho_k] =$$

$$\begin{cases} \Pr(\rho_k \in \mathbf{X}_{\mathbf{b}_m}) = 2^{(k \bmod 23) - 23} \cdot (1 - p); \\ \Pr(\rho_k \in \mathbf{X}_{\mathbf{u}'_m}) = 2^{(k \bmod 23) - 23} \cdot p; \\ \Pr(\rho_k \in [0, 1) \setminus \mathbf{X}_{\mathbf{b}_m} \setminus \mathbf{X}_{\mathbf{u}'_m}) = 1 - 2^{(k \bmod 23) - 23}. \end{cases} \quad (33)$$

By substituting (32) and (33) into (31), it follows that

$$Q_{k,u_k}[\rho_k] = \begin{cases} \Pr(\rho_k \in \mathbf{X}_{\mathbf{b}_m}) = 2^{(k \bmod 23) - 23} [p(1 - q_k) + (1 - p)q_k]; \\ \Pr(\rho_k \in \mathbf{X}_{\mathbf{u}'_m}) = 2^{(k \bmod 23) - 23} [(1 - p)(1 - q_k) + pq_k]; \\ \Pr(\rho_k \in [0, 1) \setminus \mathbf{X}_{\mathbf{b}_m} \setminus \mathbf{X}_{\mathbf{u}'_m}) = 1 - 2^{(k \bmod 23) - 23}. \end{cases} \quad (34)$$

Then, we can rewrite $\mathbb{E}_{\rho_k \sim Q_{k,u'_k}} \left(\frac{Q_{k,u_k}[\rho_k]}{Q_{k,u'_k}[\rho_k]} \right)^\lambda$ as

$$\begin{aligned} \mathbb{E}_{\rho_k \sim Q_{k,u'_k}} \left(\frac{Q_{k,u_k}[\rho_k]}{Q_{k,u'_k}[\rho_k]} \right)^\lambda &= \Pr(\rho_k \in \mathbf{X}_{\mathbf{b}_m}) \left(\frac{Q_{k,u_k}[\rho_k]}{Q_{k,u'_k}[\rho_k]} \right)^\lambda + \Pr(\rho_k \in \mathbf{X}_{\mathbf{u}'_m}) \left(\frac{Q_{k,u_k}[\rho_k]}{Q_{k,u'_k}[\rho_k]} \right)^\lambda \\ &\quad + \Pr(\rho_k \in [0, 1) \setminus \mathbf{X}_{\mathbf{b}_m} \setminus \mathbf{X}_{\mathbf{u}'_m}) \left(\frac{Q_{k,u_k}[\rho_k]}{Q_{k,u'_k}[\rho_k]} \right)^\lambda \end{aligned} \quad (35a)$$

$$= (1 - 2^{(k \bmod 23) - 23}) + 2^{(k \bmod 23) - 23} p \cdot ((1 - q_k) + q_k \frac{1-p}{p})^\lambda + 2^{(k \bmod 23) - 23} (1 - p) \cdot ((1 - q_k) + q_k \frac{p}{1-p})^\lambda \quad (35b)$$

$$\leq (1 - 2^{(k \bmod 23) - 23}) + 2^{(k \bmod 23) - 23} ((1 - q_k) + q_k \cdot \frac{(1-p)^{\lambda-1}}{p^{\lambda-1}}) \quad (35c)$$

$$= 1 - 2^{(k \bmod 23) - 23} q_k \left(\frac{(1-p)^{\lambda-1}}{p^{\lambda-1}} - 1 \right), \quad (35d)$$

where (35a) is the expansion of $\mathbb{E}_{\rho_k \sim Q_{k,u'_k}} \left(\frac{Q_{k,u_k}[\rho_k]}{Q_{k,u'_k}[\rho_k]} \right)^\lambda$, (35b) is obtain by substituting (34) and (32) in (35a), and (35c) is due to the following inequality,

$$\begin{aligned} p \cdot ((1 - q_k) + q_k \cdot \frac{1-p}{p})^\lambda + (1 - p) \cdot ((1 - q_k) + q_k \cdot \frac{p}{1-p})^\lambda \\ \leq (1 - q_k) + q_k \cdot \frac{(1-p)^{\lambda-1}}{p^{\lambda-1}}, \end{aligned} \quad (36)$$

which holds under the conditions $0 < q_k < 1$, $0 < p < 0.5$, and $\lambda > 1$ and can be verified numerically.

By substituting (35d) into (30), the Rényi divergence can be upper-bounded by

$$D_\lambda \left(Q_{k,u_k}[\rho_k] \parallel Q_{k,u'_k}[\rho_k] \right) \leq \frac{q_k 2^{(k \bmod 23) - 23}}{\lambda - 1} \left(\frac{(1-p)^{\lambda-1}}{p^{\lambda-1}} - 1 \right). \quad (37)$$

Substituting (37) into (29), the upper bound on the divergence for the entire bitstream over all bits $\forall k = 1, \dots, 23M$ can be rewritten as

$$\begin{aligned} D_\lambda(Q_{\mathbf{u}} \parallel Q_{\mathbf{u}'}) &\leq \frac{1}{\lambda - 1} \sum_{k=1}^{23M} q_k 2^{(k \bmod 23) - 23} \left(\frac{(1-p)^{\lambda-1}}{p^{\lambda-1}} - 1 \right) \\ &= \frac{\bar{\kappa} \Delta \omega_{\max, n}}{\lambda - 1} \left(\frac{(1-p)^{\lambda-1}}{p^{\lambda-1}} - 1 \right), \end{aligned}$$

where $\sum_{k=1}^{23M} q_k 2^{(k \bmod 23) - 23} = \bar{\kappa} \Delta \omega_{\max, n}$ is the expected bit-level distance, as defined in (15). When $\frac{\bar{\kappa} \Delta \omega_{\max, n}}{\lambda - 1} \left(\frac{(1-p)^{\lambda-1}}{p^{\lambda-1}} - 1 \right) \leq \frac{\epsilon}{K}$, we can directly obtain (29); i.e., $(\lambda, \frac{\epsilon}{K})$ -Rényi DP is satisfied in each round.

Further, we evaluate the end-to-end BER required to ensure that the bit-flipping mechanism satisfies (λ, ϵ) -Rényi DP across all communication rounds, as given by

$$\begin{aligned} \frac{\bar{\kappa} \Delta \omega_{\max, n}}{\lambda - 1} \left(\frac{(1-p)^{\lambda-1}}{p^{\lambda-1}} - 1 \right) &\leq \frac{\epsilon}{K} \\ \Leftrightarrow p &\geq \left(1 + \left(\frac{(\lambda-1)\epsilon}{K \bar{\kappa} \Delta \omega_{\max, n}} \right)^{\frac{1}{\lambda-1}} \right)^{-1}. \end{aligned} \quad (38)$$

Note that (38) holds under the assumption of $p < \frac{1}{2}$. This completes the proof.

C. Proof of Lemma 2

We start with (20). As discussed in Section IV-A, each model element $\omega_{t,n,m}$, $m = 1, \dots, M$, is mapped into a fixed-point number, i.e., $\omega_{t,n,m} + 3 \times 2^{(c_{30}c_{29} \dots c_{23})_2 - 126}$ within the range $[2^{(c_{30}c_{29} \dots c_{23})_2 - 125}, 2^{(c_{30}c_{29} \dots c_{23})_2 - 124}]$. After superimposing the artificial and communication bit-flipping noise, the demodulated value is still within the above range, given the error-free exponent and sign parts. Based on (5), the expectation of the demodulated value is

$$(1-2p_{t,n})(\omega_{t,n,m} + 3 \times 2^{(c_{30}c_{29} \dots c_{23})_2 - 126}) + 2^{(c_{30}c_{29} \dots c_{23})_2 - 125} \left(2p_{t,n} + \sum_{i=1}^{23} 2^{-i} p_{t,n} \right). \quad (39)$$

After reversing the mapping operation, the expectation of the finally recovered model parameter is given by

$$\mathbb{E}(\tilde{\omega}_{t,n,m}) = (1-2p_{t,n})\omega_{t,n,m} - p_{t,n} \times 2^{(c_{30}c_{29} \dots c_{23})_2 - 125} \times 2^{-23} \approx (1-2p_{t,n})\omega_{t,n,m}.$$

Here, $p_{t,n} \times 2^{(c_{30}c_{29} \dots c_{23})_2 - 125} \times 2^{-23} \ll (1-2p_{t,n})\omega_{t,n,m}$ is negligibly smaller than $(1-2p_{t,n})\omega_{t,n,m}$, leading to (20).

Next, we prove (21). Since each element in the demodulated model parameters is within the same range $[2^{(c_{30}c_{29} \dots c_{23})_2 - 125}, 2^{(c_{30}c_{29} \dots c_{23})_2 - 124}]$ and the mapping operation does not affect the randomness, from (6), the variance of each element is

$$\mathbb{E}(\tilde{\omega}_{t,n,m} - \mathbb{E}(\tilde{\omega}_{t,n,m}))^2 = \frac{(1-4^{-23})}{3} \times p_{t,n}(1-p_{t,n})2^{2(c_{30}c_{29} \dots c_{23})_2 - 250}. \quad (41)$$

Based on the definition of ℓ_2 -norm and (18), we have

$$\mathbb{E}(\|z_{t,n} - \mathbb{E}(z_{t,n})\|_2^2) = \sum_{m=1}^M \mathbb{E}(\tilde{\omega}_{t,n,m} - \mathbb{E}(\tilde{\omega}_{t,n,m}))^2, \quad (42)$$

where (42) is obtained because the random values, $\tilde{\omega}_{t,n,m}, \forall m$, are independent. By plugging (41) into (42), we obtain (21).

Then, we prove (22), as given by

$$\mathbb{E}(\|z_{t,G}\|_2^2) = \|\mathbb{E}(z_{t,G})\|_2^2 + \mathbb{E}(\|z_{t,G} - \mathbb{E}(z_{t,G})\|_2^2) \quad (43a)$$

$$\leq \sum_{n \in \mathcal{N}} q_n \|\mathbb{E}(z_{t,n})\|_2^2 + \sum_{n \in \mathcal{N}} q_n^2 \mathbb{E}(\|z_{t,n} - \mathbb{E}(z_{t,n})\|_2^2) \quad (43b)$$

$$\leq \sum_{n \in \mathcal{N}} q_n p_{t,n}^2 \nu_2^2 + \frac{(1-4^{-23})M}{3} \sum_{n \in \mathcal{N}} q_n^2 p_{t,n}(1-p_{t,n}) \times 2^{2(c_{30}c_{29} \dots c_{23})_2 - 250}, \quad (43c)$$

where (43a) is based on $\mathbb{E}(\|a\|_2^2) = \mathbb{E}(\|a - \mathbb{E}[a]\|_2^2) + \|\mathbb{E}[a]\|_2^2$ with $a = z_{t,G}$. (43b) is obtained by applying Cauchy's inequality to $\|\mathbb{E}(z_{t,G})\|_2^2$ and then exploiting the equality between the sum variance of independent variables $\{z_{t,n}, \forall n\}$ and the variance of their sum. (43c) is obtained by substituting (20) and (21) into (43b) and applying $|\omega_{t,n,m}| \leq \nu_\infty \leq 2^{(c_{30}c_{29} \dots c_{23})_2 - 126}, \forall m$. (43c) can be rewritten as (22).

D. Proof of Theorem 2

Referring to [41, Eq. (11)], we have

$$\|\bar{\omega}_t - \mathbf{w}^*\|_2^2 \leq (1-\eta\mu)\|\bar{\omega}_{t-1} - \mathbf{w}^*\|_2^2 + \eta^2 B, \quad \forall t, \quad (44)$$

where no bit-flipping DP noise is considered and $B = 6\alpha\Gamma + 8(E-1)^2 G^2$ full-batch gradient descent with $\sigma_n = 0, \forall n$.

When taking the bit-flipping DP noise into account, the one-step upper bound of $\|\bar{\omega}_t - \mathbf{w}^*\|_2^2, \forall t$ is given by

$$\forall t \notin \mathcal{I}_E : \|\bar{\omega}_t - \mathbf{w}^*\|_2^2 \leq (1-\eta\mu)\|\bar{\omega}_{t-1} - \mathbf{w}^*\|_2^2 + \eta^2 B; \quad (45a)$$

$$\forall t \in \mathcal{I}_E : \mathbb{E}(\|\bar{\omega}_t - \mathbf{w}^*\|_2^2) \leq (1+\sqrt{p_{\max}}) \times \left[(1-\eta\mu)\|\bar{\omega}_{t-1} - \mathbf{w}^*\|_2^2 + \eta^2 B + \frac{X_t^{\text{BF}}}{\sqrt{p_{\max}}} \right], \quad (45b)$$

where (45a) is obtained by plugging $\bar{\omega}_t = \bar{\omega}_t, t \notin \mathcal{I}_E$ in (44). As for (45b), $\bar{\omega}_t = \bar{\omega}_t + z_{t,G}$ when $t = kE \in \mathcal{I}_E$; thus,

$$\mathbb{E}(\|\bar{\omega}_t - \mathbf{w}^*\|_2^2) = \mathbb{E}(\|\bar{\omega}_t + z_{t,G} - \mathbf{w}^*\|_2^2) \leq (1+\sqrt{p_{\max}})\|\bar{\omega}_t - \mathbf{w}^*\|_2^2 + (1+\frac{1}{\sqrt{p_{\max}}})\mathbb{E}(\|z_{t,G}\|_2^2), \quad (46)$$

where the expectation is taken to capture the randomness of bit-flipping noise in the k -th communication round. By substituting (22) and (44) in (46), we obtain (45b).

By substituting (45a) for $t = kE+i, \dots, kE+1$ into $\|\bar{\omega}_{kE+i} - \mathbf{w}^*\|_2^2$ and using mathematical induction, it follows that

$$\|\bar{\omega}_{kE+i} - \mathbf{w}^*\|_2^2 \leq (1-\eta\mu)^i \|\bar{\omega}_{kE} - \mathbf{w}^*\|_2^2 + \eta^2 B \frac{1-(1-\eta\mu)^i}{\eta\mu}. \quad (47)$$

Then, we can obtain the upper bound of $\mathbb{E}(\|\bar{\omega}_T - \mathbf{w}^*\|_2^2)$ as

$$\mathbb{E}(\|\bar{\omega}_T - \mathbf{w}^*\|_2^2) \leq (1+\sqrt{p_{\max}}) \left[(1-\eta\mu)\mathbb{E}(\|\bar{\omega}_{T-1} - \mathbf{w}^*\|_2^2) + \eta^2 B + \frac{X_T^{\text{BF}}}{\sqrt{p_{\max}}} \right] \quad (48a)$$

$$\leq (1+\sqrt{p_{\max}}) \left[(1-\eta\mu)^E \mathbb{E}(\|\bar{\omega}_{T-E} - \mathbf{w}^*\|_2^2) + \eta^2 B \frac{1-(1-\eta\mu)^E}{\eta\mu} + \frac{X_T^{\text{BF}}}{\sqrt{p_{\max}}} \right] \quad (48b)$$

$$\leq (1+\sqrt{p_{\max}})^K (1-\eta\mu)^T \|\bar{\omega}_0 - \mathbf{w}^*\|_2^2 + \sum_{\forall i \leq K} (1-\eta\mu)^{(i-1)E} (1+\sqrt{p_{\max}})^i \left(\eta^2 B \frac{1-(1-\eta\mu)^E}{\eta\mu} + \frac{X_{iE}^{\text{BF}}}{\sqrt{p_{\max}}} \right) \quad (48c)$$

$$\leq \frac{1 - ((1-\eta\mu)^E (1+\sqrt{p_{\max}}))^K}{1 - (1-\eta\mu)^E (1+\sqrt{p_{\max}})} (1+\sqrt{p_{\max}}) \left(\eta^2 B \frac{1-(1-\eta\mu)^E}{\eta\mu} + \frac{X^{\text{BF}}}{\sqrt{p_{\max}}} \right) + (1+\sqrt{p_{\max}})^K (1-\eta\mu)^T \|\bar{\omega}_0 - \mathbf{w}^*\|_2^2, \quad (48d)$$

where (48a) is based on (45b). (48b) is obtained by substituting (47) with $t = T-1$ into (48a). Iterating (48b) for $t = KE, (K-1)E, \dots, E$ yields (48c). Eventually, (48d) is based on the definition $X^{\text{BF}} = \max_{\forall t} X_t^{\text{BF}}$.

REFERENCES

- [1] X. Tang *et al.*, "Pile: Robust privacy-preserving federated learning via verifiable perturbations," *IEEE Trans. Dependable Secure Comput.*, pp. 1–18, 2023.
- [2] J. Zhou *et al.*, "A differentially private federated learning model against poisoning attacks in edge computing," *IEEE Trans. Dependable Secure Comput.*, vol. 20, no. 3, pp. 1941–1958, 2023.
- [3] R. Bassily, A. Smith, and A. Thakurta, "Private empirical risk minimization: Efficient algorithms and tight error bounds," in *Proc. 55th Annual Symposium on Foundations of Computer Science*, 2014, pp. 464–473.
- [4] M. Abadi, A. Chu, I. Goodfellow *et al.*, "Deep learning with differential privacy," in *Proc. ACM Conf. Comput. Commun. Secur.*, New York, USA, 2016, p. 308–318.
- [5] F. Chollet, "Xception: Deep learning with depthwise separable convolutions," in *Proc. IEEE Conf. Comput. Vis. Pattern Recognit.*, 2017, pp. 1251–1258.
- [6] G. Barthe and B. Kopf, "Information-theoretic bounds for differentially private mechanisms," in *Proc. IEEE 24th Comput. Secur. Foundations Symp. (CSF)*, 2011, pp. 191–204.
- [7] G. Acs, L. Melis, C. Castelluccia, and E. De Cristofaro, "Differentially private mixture of generative neural networks," *IEEE Trans. Knowl. Data Eng.*, vol. 31, no. 6, pp. 1109–1121, 2018.

- [8] I. Mironov, "Rényi differential privacy," in *Proc. IEEE 30th Comput. Secur. Foundations Symp. (CSF)*, Aug. 2017.
- [9] T. Zhu, G. Li, W. Zhou, and S. Y. Philip, "Differentially private data publishing and analysis: A survey," *IEEE Trans. Knowl. Data Eng.*, vol. 29, no. 8, pp. 1619–1638, 2017.
- [10] Y. Fu *et al.*, "On the practicality of differential privacy in federated learning by tuning iteration times," *arXiv preprint arXiv:2101.04163*, 2021.
- [11] C. Dong *et al.*, "Privacy-preserving and byzantine-robust federated learning," *IEEE Trans. Dependable Secure Comput.*, pp. 1–16, 2023.
- [12] Y. Zhao *et al.*, "Local differential privacy based federated learning for internet of things," *IEEE Internet Things J.*, pp. 1–1, 2020.
- [13] D. Liu and O. Simeone, "Privacy for free: Wireless federated learning via uncoded transmission with adaptive power control," *IEEE J. Sel. Areas Commun.*, vol. 39, no. 1, pp. 170–185, 2021.
- [14] K. Wei *et al.*, "Federated learning with differential privacy: Algorithms and performance analysis," *IEEE Trans. Inf. Forensics Secur.*, vol. 15, pp. 3454–3469, 2020.
- [15] X. Yuan, W. Ni, M. Ding *et al.*, "Amplitude-varying perturbation for balancing privacy and utility in federated learning," *IEEE Trans. Inf. Forensics Secur.*, vol. 18, pp. 1884–1897, 2023.
- [16] A. Hansen and M. Nelkin, "Nyquist noise in a fractal resistor network," *Physical Review B*, vol. 33, no. 1, p. 649, 1986.
- [17] Z. Zhang *et al.*, "Communication and energy efficient wireless federated learning with intrinsic privacy," *IEEE Trans. Dependable Secure Comput.*, vol. 21, no. 4, pp. 4035–4047, 2024.
- [18] M. Salehi and E. Hossain, "Federated learning in unreliable and resource-constrained cellular wireless networks," *IEEE Trans. Commun.*, vol. 69, no. 8, pp. 5136–5151, Aug. 2021.
- [19] S. Chen, D. Yu *et al.*, "Decentralized wireless federated learning with differential privacy," *IEEE Trans. Industrial Informatics*, vol. 18, no. 9, pp. 6273–6282, 2022.
- [20] P. Lai, H. Phan, L. Xiong, K. Tran, M. Thai, T. Sun, F. Deroncourt, J. Gu, N. Barmpalios, and R. Jain, "Bit-aware randomized response for local differential privacy in federated learning," 2022.
- [21] *IEEE Standard for Floating-Point Arithmetic*, 2019.
- [22] S. M. Shah and V. K. N. Lau, "Model compression for communication efficient federated learning," *IEEE Trans. Neural Netw. Learn. Syst.*, vol. 34, no. 9, pp. 5937–5951, 2023.
- [23] L. Liu, J. Zhang, S. Song, and K. B. Letaief, "Hierarchical federated learning with quantization: Convergence analysis and system design," *IEEE Trans. Wireless Commun.*, vol. 22, no. 1, pp. 2–18, 2023.
- [24] X. Su, Y. Zhou, L. Cui *et al.*, "On model transmission strategies in federated learning with lossy communications," *IEEE Trans. Parallel Distrib. Syst.*, vol. 34, no. 4, pp. 1173–1185, Apr. 2023.
- [25] T. Sery and K. Cohen, "On analog gradient descent learning over multiple access fading channels," *IEEE Trans. Signal Process.*, vol. 68, pp. 2897–2911, 2020.
- [26] X. Yu, B. Xiao, W. Ni, and X. Wang, "Optimal adaptive power control for over-the-air federated edge learning under fading channels," *IEEE Trans. Commun.*, vol. 71, no. 9, pp. 5199–5213, 2023.
- [27] J. Yao, Z. Yang, W. Xu, D. Niyato, and X. You, "Imperfect csi: A key factor of uncertainty to over-the-air federated learning," *IEEE Wireless Commun. Lett.*, vol. 12, no. 12, pp. 2273–2277, 2023.
- [28] N. Lang *et al.*, "Joint privacy enhancement and quantization in federated learning," *IEEE Trans. Signal Process.*, vol. 71, pp. 295–310, 2023.
- [29] A. Koloskova *et al.*, "Revisiting gradient clipping: Stochastic bias and tight convergence guarantees," in *Proc. 40th Int. Conf. Machine Learning*, vol. 202, 23–29 Jun 2023, pp. 17343–17363.
- [30] H. Lee *et al.*, "On defensive neural networks against inference attack in federated learning," in *Proc. IEEE Int. Conf. Commun. (ICC)*, Montreal, QC, Canada, 2021, pp. 1–6.
- [31] S. K. Rao *et al.*, "A survey on advanced encryption standard," *Int. J. Science and Research*, vol. 6, no. 1, pp. 711–724, 2017.
- [32] P. Matta *et al.*, "A comparative survey on data encryption techniques: Big data perspective," in *Proc. ICAMM*, vol. 46, 2021, pp. 11035–11039.
- [33] A. Acar *et al.*, "A survey on homomorphic encryption schemes: Theory and implementation," *ACM Computing Surveys (Csur)*, vol. 51, no. 4, pp. 1–35, 2018.
- [34] M. Simon and M. Alouini, *Digital Communication over Fading Channels*, ser. Wiley Series in Telecommunications and Signal Processing. Wiley, 2005. [Online]. Available: <https://books.google.com.au/books?id=OYrDNOQ6BacC>
- [35] A. Goldsmith, *Wireless Communications*. Cambridge University Press, 2005.
- [36] C. Dwork, A. Roth *et al.*, "The algorithmic foundations of differential privacy," *Foundations and Trends® in Theoretical Computer Science*, vol. 9, no. 3–4, pp. 211–407, 2014.
- [37] I. Mironov, K. Talwar, and L. Zhang, "Rényi differential privacy of the sampled gaussian mechanism," *CoRR*, vol. abs/1908.10530, 2019. [Online]. Available: <http://arxiv.org/abs/1908.10530>
- [38] T. Tuor *et al.*, "Distributed machine learning in coalition environments: Overview of techniques," in *Proc. Int. Conf. Info. Fusion (FUSION)*, July 2018, pp. 814–821.
- [39] W. Li, T. Lv, W. Ni *et al.*, "Decentralized federated learning over imperfect communication channels," *IEEE Trans. Commun.*, vol. 72, no. 11, pp. 6973–6991, 2024.
- [40] S. U. Stich, "Local SGD converges fast and communicates little," in *International Conference on Learning Representations*, 2019.
- [41] X. Li, K. Huang, W. Yang *et al.*, "On the convergence of fedavg on Non-IID data," in *Proc. ICLR*, 2020.
- [42] K. He, X. Zhang, S. Ren *et al.*, "Deep residual learning for image recognition," in *Proc. IEEE/CVF Conf. Comput. Vis. Pattern Recognit. (CVPR)*, Las Vegas, US, June 2016.
- [43] C. L. Canonne, G. Kamath, and T. Steinke, "The discrete gaussian for differential privacy," *arXiv preprint arXiv:2004.00010*, 2021.



Weicai Li (Graduate Student Member, IEEE) received the B.E. degree in communication engineering from Beijing University of Posts and Telecommunications (BUPT), China, in 2020. She is pursuing her Ph.D. with the School of Information and Communication Engineering at BUPT. From December 2022 to December 2023, she was a Visiting Scholar at the University of Technology Sydney. Her research interests include wireless federated learning, privacy computing, and semantic communication.



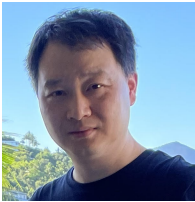
Tiejun Lv (Senior Member, IEEE) received the M.S. and Ph.D. degrees in electronic engineering from the University of Electronic Science and Technology of China (UESTC), Chengdu, China, in 1997 and 2000, respectively. From January 2001 to January 2003, he was a Postdoctoral Fellow at Tsinghua University, Beijing, China. In 2005, he was promoted to Full Professor at the School of Information and Communication Engineering, Beijing University of Posts and Telecommunications (BUPT). From September 2008 to March 2009, he was a Visiting Professor with the Department of Electrical Engineering at Stanford University, Stanford, CA, USA. He is the author of four books, one book chapter, more than 160 published journal papers and 200 conference papers on the physical layer of wireless mobile communications. His current research interests include signal processing, communications theory and networking. He was the recipient of the Program for New Century Excellent Talents in University Award from the Ministry of Education, China, in 2006. He received the Nature Science Award from the Ministry of Education of China for the hierarchical cooperative communication theory and technologies in 2015. He has won best paper award at CSPA 2022. Dr. Lv has been an Editor for Sensors since 2024.



Xiyu Zhao received the B.E. degree in communication engineering from Beijing University of Posts and Telecommunications (BUPT), China, in 2020. She is pursuing her Ph.D. with the School of Information and Communication Engineering at BUPT. From June 2023 to December 2024, she was a Visiting Scholar at Macquarie University. Her research interests include wireless federated learning, distributed computing, and privacy-preserving.



Xin Yuan received the Ph.D. degree in communication engineering from Beijing University of Posts and Telecommunications (BUPT), China, in 2019. Her research interests include wireless federated learning, distributed computing, and privacy-preserving.



Wei Ni is a Mechatronics Program Advisor and Professor (Honorary) at Macquarie University, Sydney, New South Wales, Australia. His research interests include channel modeling, communications and signal processing, array signal processing, networking, multiple access, modulation and coding, radio access network (RAN), resource allocation, smart grid, blockchain, Internet-of-Things (IoT), autonomous systems, cyber-physical systems (CPS), and connected intelligent systems in general.